



1 **On the role of trans-lithospheric faults in the long-term**
2 **seismotectonic segmentation of active margins: a case study**
3 **in the Andes**

4
5 Gonzalo Yanez C.¹, Jose Piquer R.², Orlando Rivera H.³

6
7 ¹ Pontificia Universidad Católica de Chile, Av. Vicuña Mackenna 4860, Macl, Santiago, Chile, gyaneza@uc.cl

8 ² Instituto de Ciencias de la Tierra, Universidad Austral de Chile, jose.piquer@uach.cl

9 ³ Minera Peñoles de Chile, orlando_rivera@penoles.com.mx

10 *Correspondence to:* Gonzalo Yanez C. (gyaneza@uc.cl)

11 **Abstract.** Plate coupling play a fundamental role in the way in which seismic energy is released during the
12 seismic cycle. This process includes quasi-instantaneous release during megathrust earthquakes and long-term
13 creep. Both mechanisms can coexist in a given subducting margin, defining a seismotectonic segmentation in
14 which seismically active segments are separated by zones in which ruptures stop, classified for simplicity as
15 asperities and barrier, respectively. The spatiotemporal stability of this segmentation has been a matter of debate
16 in the seismological community for decades. At this regard, we explore in this paper the potential role of the
17 interaction between geological heterogeneities in the overriding plate and fluids released from the subducting
18 slab towards the subduction channel. As a case study, we take the convergence between the Nazca and South
19 American plates between 18°-40° S, given its relatively simple convergence style and the availability of a high-
20 quality instrumental and historical record. We postulate that trans-lithospheric faults striking at a high angle
21 with respect to the trench behave as large fluid sinks that create the appropriate conditions for the development
22 of barriers and promote the growth of highly coupled asperity domains in their periphery. We tested this
23 hypothesis against key short- and long-term observations in the study area, obtaining consistent results. If the
24 spatial distribution of asperities is controlled by the geology of the overriding plate, seismic risk assessment
25 could be established with better confidence.

26
27

28 **1 Introduction**

29 Subduction margins accommodate short-term (years to tens of years) and long-term (thousands to millions of
30 years) deformation. The most evident effects of these two deformational behaviours are earthquakes (short-
31 term) and mountain-building (long-term) (e.g. Avouac, 2007). The concept of the seismic cycle, introduced by
32 Fedotov (1968) and further elaborated by Mogi (1977, 1985), identifies two stages: a long inter-seismic period
33 (several tens of years), followed by a short co-seismic period (minutes at most) where the elastic energy stored



34 during the previous stage is released as an earthquake. For earthquake magnitudes in the range of M_w 7.5–9.5,
35 the observed mean slip displacement varies from 0.8–10 meters (Thingbaijam et al., 2017). Even though the
36 maximum mean slip in megathrust events is 10 meters, the zones of maximum slip, equated to asperities (e.g.,
37 Aki, 1984, Lay & Bileck 2007, Lay 2015) can reach 20–40 meters in wavelength patches in the range of 20–
38 100 kilometres (see, e.g., <http://equake-rc.info/srcmod/>). However, the release of elastic energy during the
39 seismic cycle only accounts for 90–95% of the deformation accumulated interseismically in convergent margins;
40 the remaining 5–10% produces permanent deformation in the overriding plate, expressed as crustal shortening
41 and mountain building (e.g. Yañez and Cembrano, 2004). This long-term process lasts for hundreds to
42 thousands of seismic cycles (time windows of millions of years). Therefore, both phenomena — earthquakes
43 and mountain building — are extreme responses to the same process: the convergence between oceanic and
44 continental plates, including the development of asperities and barriers in the same spatial and time frame.

45 The concepts of asperities and barriers were proposed by Lay et al. (1982) and Aki (1984) to describe the
46 process during the occurrence of an earthquake and intimately related to the concept of plate coupling. More
47 recent studies (e.g. Bileck and Lay, 2007) propose a more complex mechanism at the subduction plate contact,
48 in which domains of unstable stick-slip state coexist with other domains in a conditionally stable stick-slip state,
49 and zones that develop aseismic slip/stable behaviour. These three states — unstable, conditionally stable, and
50 stable stick-slip behaviour — represent different slip modes that can be represented as asperities and barriers in
51 the old nomenclature. However, the conceptualization of Bileck and Lay (2007) proposes an along-dip (depth)
52 distribution of the different slip behaviours: (1) aseismic-stable at depths of 5–10 kilometres, (2) mostly
53 conditionally stable at depths of 10–15 kilometres, and (3) unstable stick-slip behaviour (Brace and Byerlee
54 (1966) and Burridge and Knopoff (1967)) at depths of 15–25 kilometres. Recent studies on exhumed subduction
55 domains in California (Platt et al., 2018) corroborate this along-dip transition from seismic zone to transition
56 zone. One interesting characteristic of these domains is that unstable domains are generally surrounded by
57 conditionally stable domains and aseismic domains in their outermost periphery.

58 To date, there is no clear evidence on whether the geological/tectonic process(es) control to some extent these
59 seismogenic behaviours and/or their stability across several seismic cycles or geological time frames. Potential
60 candidates already proposed include: (1) the roughness of the subducting plate (aseismic ridges, fracture zones,
61 horst/graben structures, etc.) (e.g. Bilek et al., 2003, Wang and Bilek, 2011; Gersen et al., 2015; Philibosian and
62 Meltzner, 2020; Molina et al., 2021); (2) fluid-controlled overpressure (Peacock, 1990; Safer and Tobin, 2011;
63 Safer, 2017; Menant et al., 2019); (3) the shape of the subducting plate (e.g. Gutscher et al., 1999); (4) the
64 geology of the overriding plate (i.e. Kimura et al., 2018; Philibosian and Meltzner, 2020; Molina et al., 2021),
65 among others, including various combinations of these different possible factors.

66 The role of fluids released from the subducting slab has emerged as a first-order factor in the plate-coupling
67 processes at subduction margins. Direct observations (e.g., Saffer and Tobin, 2011; Tsuji et al., 2014) and
68 numerical modelling (Menant et al., 2019) demonstrate that fluids released from the subducting oceanic crust
69 and subduction channel define segments at the plate-coupling zone with distinct pore pressure characteristics.
70 Overpressure domains are associated with zones of weak coupling, and strong coupling is observed in the case
71 of zones showing low pore pressure behaviour. The first type of domain is in direct association with creep zones



72 or slow slip events, while the other one is in direct association with locked zones, or in the seismological
73 nomenclature, the barrier and asperity domains, respectively. Seismic imaging of the forearc wedge (e.g. Tsuji
74 et al., 2014) and numerical modelling also show that fluids percolate upwards in the zones of maximum
75 overpressure, including the emplacement of serpentinite bodies along weak zones or faults.

76

77 In this paper, we propose a causal relationship between the presence of trans-lithospheric faults (TLF) in the
78 overriding plate and seismic segmentation, involving the control of TLF on the movement/storage/release of
79 overpressure fluids along and across the subduction zone. We use the Central Southern Andes as a case study,
80 as it is one of the most active seismogenic sites worldwide, is well studied, and has a relatively simple
81 subduction geometry (Hayes, 2018). In addition, recent structural and geophysical mapping has revealed the
82 role of TLF in the tectono-magmatic evolution of the continental margin of this region (e.g. Yañez et al., 1988,
83 Santibáñez et al., 2019; Cembrano and Lara, 2009; Melnick and Echtler, 2006; Yañez and Rivera, 2019; Piquer
84 at al., 2019, 2021a). We aim to demonstrate that the interaction between these TLF and the fluid circulating
85 through the subduction channel provides a simple first-order explanation for the Andean seismotectonic
86 organization through a long-lived geological control.

87 **2 Data and methods**

88 **2.1 Tectonic background**

89 The Nazca-South American plate convergence is a subduction-type margin that has been active in this segment
90 of the Andes since at least the Cretaceous without the accretion of new terrains (Mpodozis and Ramos, 1990).
91 Since 15 Ma, the convergence has been slightly oblique (E10°N) at a velocity of around 6.5 cm/yr (Angermann
92 et al., 1999). The age of the oceanic plate varies between 0 Ma at the triple junction of Taitao (44°S) to 45 Ma
93 at the Orocline bending of Bolivia (18°S) (Figure 1). A flat slab segment is located between 28°S and 33°S
94 latitude, affecting the development of an asthenospheric wedge landward and inhibiting the occurrence of active
95 volcanism since the last 5 Ma (Kay and Mpodozis, 2002). However, the Wadati-Benioff plane is roughly
96 homogenous in dip along the plate coupling between the Nazca and South American plates (Slab 2.0, Hayes,
97 2018). The roughness of the Nazca plate is affected by a progressively older oceanic crust northward, with some
98 fracture zones offsetting the plate, the subduction of a triple junction with an active spreading centre (now at
99 Taitao Peninsula), some episodic magmatic activity along the Juan Fernandez Ridge (33°S, Yañez et al., 2001),
100 and eventually a smaller ridge at 20°S (Perdida Ridge, Cahill and Isacks, 1992). Overall, these features can be
101 described as minor obstacles to the subduction of a relatively young oceanic plate underneath a continental plate
102 in a highly coupled convergence margin (Section 2.5).

103

104 **2.2 Compilation of trans-lithospheric faults in the Andean active margin and their role as long-lived** 105 **high-permeability domains**



106 Trans-lithospheric faults (TLF) correspond to long-lived, high-angle fault systems, which have been identified
107 in several segments of the Andean margin, based on geological mapping (e.g. Santibañez et al. 2019; Cembrano
108 and Lara, 2009; Melnick and Echtler, 2006; Piquer et al., 2021a; Farrar et al., 2023; Wiemer et al., 2023), crustal
109 seismicity (e.g. Talwani, 2014.), a combination of indirect geophysical techniques (Yañez et al., 1998), or a
110 combination of all of these (Yañez and Rivera, 2019; Piquer et al., 2019; Pearce et al., 2020).

111 In Table 1 we present a synthesis of the current status of knowledge regarding TLF definition and the major
112 geological/geophysical evidences that described them. The number assigned in each case is used later on in
113 Figure 1 as an identificatory.

114 Detailed structural mapping in various segments of the Andean margin has provided direct geological evidence
115 for the presence of TLF. They are manifested in the field as networks of individual high-angle faults, defining
116 deformation zones with widths of up to several kilometres, and lengths in the order of hundreds of kilometres,
117 being possible to follow their trace across the entire continental margin (Lanza et al., 2013; Yañez and Rivera,
118 2019; Piquer et al., 2021a). These fault networks correspond to the expression at the present-day surface of a
119 pre-existing TLF, as a result of its vertical propagation through Mesozoic and Cenozoic igneous and
120 sedimentary rocks (McCuaig and Hronsky, 2014; Piquer et al., 2019). Field observations also show that,
121 consistent with their high dip angle (commonly $>60^\circ$ and in several cases sub-vertical, although individual fault
122 segments can dip at slightly lower angles), TLF tend to be reactivated as basin-bounding faults during
123 extensional episodes, and are thus associated with violent changes in the stratigraphic record (Piquer et al.,
124 2015, 2021a; Yañez and Rivera, 2019). They also control the distribution of exhumed basement blocks (Yañez
125 and Rivera, 2019).

126 The geological record demonstrates that TLF are long-lived structures, which have played a major role in the
127 long-term evolution of the Chilean continental margin, being reactivated with different kinematics under
128 varying tectonic regimes. It is likely that several TLF were originated in the Proterozoic and the Palaeozoic
129 (Yañez and Rivera, 2019); there is strong geological evidence suggesting the present-day TLF architecture was
130 already in place by the Permo-Triassic, a period in which these structures acted as master and transfer faults for
131 intra-continental rift systems (Niemeyer et al., 2004; Sagripanti et al., 2014; Espinoza et al., 2019). Syn-tectonic
132 emplacement of magma along TLF has been documented at least since the Jurassic (Creixell et al., 2011).

133 Geophysical support for the TLF architecture in the continental margin is provided by the geometry of magnetic
134 and gravimetric anomalies (Piquer et al., 2019; Yañez and Rivera, 2019) and also by magnetotelluric data
135 (Pearce et al., 2020) and seismic tomography (Yañez and Rivera, 2019). Evidence of seismic activity in some
136 of these TLF has been recorded, for example, a precursory event to the 9.3 Mw 1960 Valdivia Earthquake
137 (Lanahue fault, Melnick et al., 2009), and the coseismic rebound associated with the 8.8 Mw 2010 Maule
138 earthquake (Pichilemu fault, e.g. Farías et al., 2011; Aron et al., 2013). Additionally, researchers have
139 documented a strong spatial relationship between a TLF and a major seismic swarm (Valparaíso seismic
140 sequence of 2017, Nealy et al., 2017) at the subduction megathrust (Piquer et al., 2021a).

141 Regarding the role of TLF as long-lived high-permeability domains, Yañez and Rivera (2019) postulated that
142 they represent weak lithospheric domains that favour fluid flow and the emplacement of different types of ore
143 deposits over large time periods (tens of millions of years), beginning with stratabound and IOCG-type deposits



144 in the Jurassic. A similar conclusion has been reached by Farrar et al. (2023) for the emplacement of porphyry
145 copper deposits of various ages, and by Wiemer et al. (2023) for gold-rich superclusters of various types of
146 mineral deposits. The strong relationship between the locations of TLF and those of giant ore deposits at specific
147 metallogenic belts has been discussed more specifically in the Andes of Northern (e.g., Chernicoff et al., 2002)
148 and Central Chile (e.g., Piquer et al., 2016) and neighbouring regions in Argentina. Similarly, there is a well-
149 established relationship between the locations of TLF and volcanic/geothermal activity in the Andes of Southern
150 Chile (e.g., Cembrano and Lara, 2009). Moreover, high Vp/Vs ratios that were documented during the
151 Pichilemu seismic sequence following the 2010 Maule earthquake have been interpreted as strong evidence of
152 fluid migration (Fariñas et al., 2011).

153 Various authors have discussed how the type of magmatic-hydrothermal product and fluid flow regime varies
154 depending on the orientation of a specific high-angle fault system (in several cases, a TLF) relative to the
155 predominant stress tensor (Lara et al., 2006; Cembrano and Lara, 2009; Roquer et al., 2017; Piquer et al.,
156 2021b). Of particular relevance is the orientation of the fault system relative to the maximum stress (σ_1); if the
157 fault system is sub-parallel or strikes at a low angle relative to σ_1 , it is well-oriented for opening and reactivation
158 respectively, allowing the rapid ascent of magma and hydrothermal fluids through different crustal segments.
159 On the other hand, if the fault system is sub-perpendicular or strikes at a high angle relative to σ_1 , it would be
160 poorly oriented or misoriented for reactivation and would promote the storage of magma and hydrothermal
161 fluids at depth (e.g. Cembrano and Lara, 2009; Stanton-Yonge et al., 2016; Piquer et al., 2021b). In the latter
162 case, a requirement for fault reactivation and the release of the accumulated fluids is that supra-lithostatic fluid
163 pressures are achieved; once this occurs, the fault system would allow the discharge of the accumulated fluids
164 towards upper crustal levels and would act as a fluid pump (“fault-valve behaviour”), concentrating fluids in
165 the fractured areas within the fault system and leading to the depletion of fluids in the surrounding regions
166 (Sibson, 1990, 2020; Cox, 2016). These fluid discharge events cause seismic swarms (Cox, 2016), which
167 concentrate at the base of the high-angle fault system (Sibson, 2020).

168 Figure 1 presents the main array of NW- and NE-striking TLF observed in the Andean margin; their seaward
169 trend has been extrapolated following the observed trend in the continental lithosphere, in particular south of
170 36°S, following the trace of submarine canyons.

171



172 Table 1: Main Trans-Lithospheric Faults of the Chilean Andes (17-42°S Latitude)

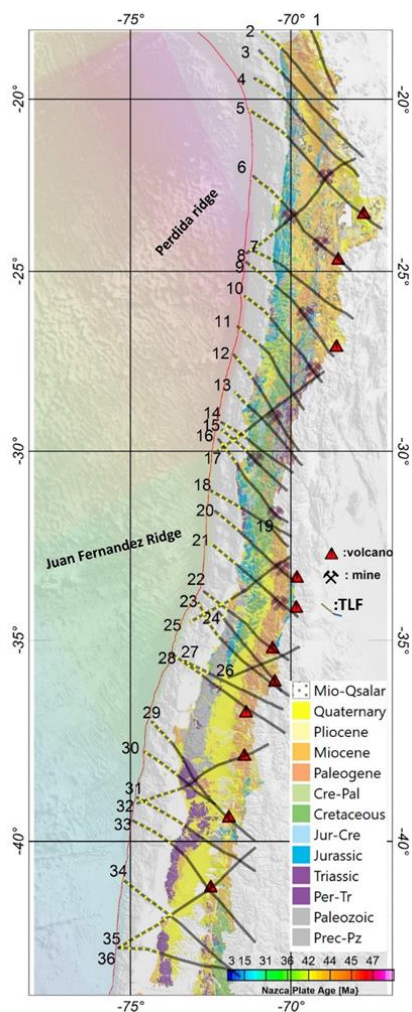
LSS_ID	LSS_NAME	REFERENCES	GEOLOGICAL EVIDENCES
1	Visviri	(15), (22)	(L)(TLS)(SC)(GVA), Antofalla Basement (T)
2	Arica	(15), (21), (22)	Arequipa Massif (T), ETL NW Arica (TLS)
3	Camarones	(22)	(TLS)(GVA)(SDGU)
4	Iquique	(22)	(TLS)(GVA)(SDGU)
5	Calama	(1), (2), (8), (20), (21), (22), (24)	Comache (F), Calama-Olapato-El Toro (L)(FS)(VA), Solá (F), Chorrillos (F), ETL NW Calama (TLS)
6	Mejillones-Llullailaco	(8), (10), (21), (22), (29)	Archibarca (L)(VA), Cataclasis de Sierra de Varas (DZ), ETL NW Mejillones (TLS)
7	Agua Verde-Exploradora	(8), (22)	Culampajá (L)
8	Antofagasta-Conchi	(22), (27), (28), (30)	Antofagasta-Calama (L)(PMG)(TR)(STMH)
9	Taltal-Potreros	(8), (22)	Taltal (L)(TLS)(SDGU)(VA)(STMH)
10	Chañaral	(8), (22)	(TLS)(GVA)(SDGU)
11	Copiapó	(22)	(TLS)(SDGU)
12	Vallenar	(22)	(TLS)(SDGU)
13	Domeyko	(22)	(TLS)(GVA)(SDGU)
14	Vicuña	(22)	(TLS)(GVA)(SDGU)
15	Andacollo	(22)	(TLS)(GVA)(SDGU)(STMH)
16	Punitaqui-Los Pelambres	(22)	(TLS)(GVA)(SDGU)(MA)(STMH)
17	El Potro	(22)	(TLS)(SDGU)
18	Illapel	(22)	(TLS)(GVA)(SDGU)
19	Almendrillo	(22)	(TLS)(GVA)(SDGU)
20	La Liga-Los Andes	(21), (22), (31)	(TLS)(GVA)(SDGU)(SC)(MA), Río Blanco-Los Bronces (FS)(STMH)
21	Valparaíso-Volcán Maipo	(3), (5), (7), (19), (21), (22), (23), (26)	Piuquencillo (F)(FS)(STMH), Melipilla (F)(MA), Marga-Marga (FS), Valparaíso-Curacaví (FS)(STMH), Concón (MDS), Cartagena (MDS), El Tabo (MDS)
22	Pichilemu	(9), (17), (22), (23), (24), (25)	Pichilemu (ATS), Tenó (FS)(SC)(STMH), Planchón-Peteroa (LLBS)(SC)
23	Laguna del Maule	(32), (33)	Río Maule (F)(VA)(SDGU)(STMH)
24	Iloca-Río Melado	(34)	Laguna Fea (FS)(VA)(STMH)
25	Aconcagua-San Antonio	(4), (6), (22), (23), (31)	Puangue (F), Estero Chacabuco (F), Estero Colina (F), El Salto (FS)(STMH)
26	Volcán Quizapu	(33)	(VA)(MDS)
27	Parral-Bullileo	This study	(VA)(SDGU)
28	San Carlos-Nevedos de Chillán	(12), (17), (18)	Chillán (AZ), Nevados de Chillán-Tromen (LLBS), Cortaderas (L)
29	Lanahue-Volcán Villarrica	(11), (14), (16), (17), (24)	Morguilla (FLS), Lanahue (F)(FS), Villarrica-Quetrupillán-Lanín (LLBS)
30	Tirúa-Pitrufquén	(11), (16)	Mocha-Villarrica (FS)
31	Río Calle Calle-Lago Ranco	(13), (17)	Carrán-Los Venados (LLBS), Futrono (F)
32	Puerto Saavedra-Volcán Callaqui	(18)	Copahue-Callaqui (AZ)
33	Osorno-Volcán Calbuco	This study	(VA)
34	Ancud-Volcán Michimahuida	(17)	Michimahuida (LLBS)
35	Cucao-Chaitén	(17)	Chaitén (LLBS)
36	Chacao-Osorno-Puntiagudo	(17)	(VA)

Abbreviations: (ATS) Andean Transverse System; (AZ) Accommodation Zone; (DZ) Deformation Zone; (F) Fault; (FLS) Fault-line Scarp; (FS) Fault System; (GVA) Gravimetric Anomaly; (L) Lineament; (LLBS) Long-Lived Basement Structures; (LLTF) Long-Lived Transverse Fault; (MA) Magnetic Anomaly; (MDS) Mafic Dike Swarm; (PMG) Paleomagnetism; (SC) Seismic Cluster; (SDGU) Structural Discontinuity of Geological Units; (T) Terrane; (TLS) Translithospheric Structures; (TR) Tectonic Rotations; (STMH) Syn-Tectonic Magmatic-Hydrothermal Centers; (VA) Volcano Alignment. **Reference Keys:** (1) Salfity, 1985; (2) Marrett et al., 1994; (3) Gana et al., 1996; (4) Wall et al., 1996; (5) Yáñez et al., 1998; (6) Wall et al., 1999; (7) Rivera & Cembrano, 2000; (8) Chernicoff et al., 2002; (9) Sernageomin, 2003; (10) Niemeyer et al., 2004; (11) Haberland et al., 2006; (12) Ramos & Kay, 2006; (13) Lara et al., 2006; (14) Glodny et al., 2008; (15) Ramos, 2008; (16) Melnick et al., 2009; (17) Cembrano & Lara, 2009; (18) Radic, 2010; (19) Creixell et al., 2011; (20) Lanza et al., 2013; (21) Rivera, 2017; (22) Yáñez & Rivera, 2019; (23) Piquer et al., 2019; (24) Santibáñez et al., 2019; (25) Pearce et al., 2020; (26) Piquer et al., 2021a; (27) Arriagada et al., 2003; (28) Peña, 2010; (29) Richards et al., 2013; (30) Palacios et al., 2007; (31) Piquer et al., 2015; (32) Kohler, 2016; (33) Fischer, 2021; (34) Torres, 2021.

173

174

175



176

177 **Figure 1: The spatial distribution of trans-lithospheric faults (TLF) over the regional geology of the Chilean**
 178 **continental margin (from SERNAGEOMIN, 2003). The traces of the TLF's are based on the models of Yáñez and**
 179 **Rivera (2019) and Piquer et al. (2019) in Northern and Central Chile, and after the model of Melnick and Ehtler**
 180 **(2006) in Southern Chile. Also shown are the locations of the main ore deposits (from north to south, Chuquicamata,**
 181 **Mantos Blancos, Escondida, Salvador, Cerro Casale, El Indio, Andacollo, Los Pelambres, Río Blanco-Los Bronces**
 182 **and El Teniente), and active volcanoes (from north to south, Láscar, Llullaillaco, Ojos del Salado, Tupungatito,**
 183 **Maipo, Planchón-Peteroa, Laguna del Maule, Chillán, Callaqui, Villarrica and Osorno) to show their**
 184 **correspondence with the TLF array. TLF are extended until the trench, following their main trend and the canyons**
 185 **trace to the south of 36°S, using segmented red lines to highlight the uncertainty of this offshore extension. In the**
 186 **seaward side of the figure, the age map of Müller et al. (2019) is included with the bathymetry of the seafloor**

187



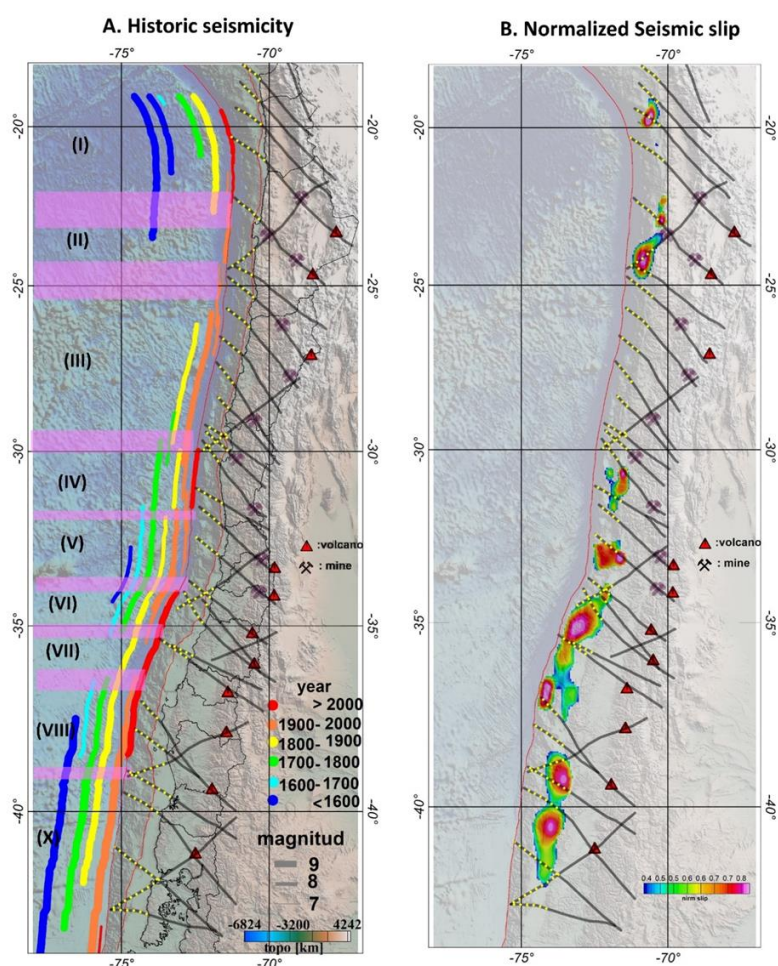
188 **2.3 Historic seismicity and Slip solutions during the last 50 years Trans-lithospheric faults (TLF)**
189 **correspond**

190 The historic seismic record in the region is short, extending from the start of the Spanish Colonization in the
191 region (present territories of Perú and Chile, circa 1500 ac). Compilations of historic seismicity and subsequent
192 interpretation to assess the magnitude and longitudinal extension of the events have been provided in Ruiz and
193 Madariaga (2018) and Scholz and Campos (2012), among others. Figure 2, panel A, includes all the historic
194 events described by these authors, as well as events above 7 Mw from the USGS catalogue. As noted by several
195 authors (Ruiz and Madariaga, 2018, and references therein), there is evidence of seismo-tectonic segmentation
196 in the historic record. For the present analysis, we define seven domains from north to south with some
197 distinctive characteristics; the boundaries between each domain are defined by a width domain of roughly 100-
198 200 kilometres that represents the uncertainty in the rupture length of the major events, wider boundaries for
199 the cases of lacking information, in particular in the northern area where the historic record is scarce Domain
200 I, in the northernmost part of the study region, shows a sequence of events close to magnitude 8 Mw and
201 separated by 100–150 years. Domain II has no large events (above 8 Mw) in the historic record, instead having
202 a series of intermediate events of magnitude 7–7.7 Mw between 1960 and 2020. Domain III has two events
203 with magnitudes in the range 8.3–8.5 Mw separated by almost 10 years, but with a current seismic gap of 100
204 years. Domain IV is less than 200 kilometres in length and includes a series of seismic events of magnitude 8
205 Mw or above. According to Ruiz and Madariaga (2018), the three major events in this domain show relatively
206 consistent recurrence times (60–80 years) and magnitudes (8–8.4 Mw), namely, the earthquakes of 2015
207 (Illapel, 8.3 Mw), 1943, and 1880. Domain V is also relatively small, about 300 km, and includes regular events
208 of around magnitude 8 Mw, including the Valparaiso 1985 8 Mw event and the 1906 8.4 Mw event. Domain
209 Vi, VII and VIII include part of the Maule 2010 8.8 Mw and Concepción 1835 8.6 Mw events, but are defined
210 as such based on some less than 8 Mw events, Domain X, the southernmost domain, is dominated by the giant
211 events of Valdivia 1960, 9.3 Mw, and 1737, 9.0 Mw.

212 Adequate seismic coverage is available since 1985 in Chile. In this period, six large earthquakes have been
213 recorded: Valparaiso 1985, 8.0 Mw (Comte et al., 1986; Mendoza et al., 1994); Antofagasta 1995, 8.0 Mw
214 (Ruegg et al., 1996; Delouis et al., 1997; Pritchard et al., 2002 and Chlieh et al., 2004); Tocopilla 2007, 7.8 Mw
215 (Schurr et al., 2012); Maule 2010, 8.8 Mw (Delouis et al., 2010; Lay et al., 2010; Vigny et al., 2011; Koper et
216 al., 2012; Ruiz et al., 2012; Moreno et al., 2012; Lorito et al., 2011; Lin et al., 2013; Yue et al., 2014); Iquique
217 2014, 8.2 Mw (Ruiz et al., 2014; Hayes et al., 2014; Schurr et al., 2014; Lay et al., 2014), and Illapel 2015, 8.3
218 Mw (Melgar et al., 2016; Heidarzadeh et al., 2016; Li et al., 2016; Lee et al., 2016; Satake and Heidarzadeh,
219 2017). Given the large size of the Valdivia 1960 earthquake (9.3 Mw), we also include slip estimates for this
220 event based on surface deformation data (Barrientos and Ward, 1990). The slip distribution of these events
221 ranges from 1 meter (e.g. Tocopilla 2007, Antofagasta 1995), several meters (e.g. Illapel 2015, Iquique 2014),
222 and more than 10 meters (Valdivia 1960, Maule 2010); however, in Figure 2, panel B, we normalize the slip



223 distribution with respect to the corresponding maximum slip in each case, plotting over the slab surface to
 224 highlight its spatial distribution. This approach aims to highlight the zones of maximum slip in each case and
 225 to appreciate their spatial and temporal distribution, under the working hypothesis that they represent the zones
 226 of maximum slip and are most likely a good proxy to identify asperities in the plate contact zone. These
 227 maximum slip zones are generally distributed between the TLF network (Figure 2).



228

229 **Figure 2:** Panel A: historical seismicity from the years 1450 to 2020 (for a full description of each event, see Table
 230 A.1 of the supplementary material). The lateral extent of each event indicates the NS estimate of the event name; the
 231 colour scale corresponds to the Mw magnitude in each case. Seismo-tectonic segmentation is indicated by yellow
 232 semi-transparent ribbons, which are extended downwards to the lower panels. Panel B: zones of maximum slip in
 233 the megathrust events registered at the margin of Chile since 1960.

234

235 2.4 Cumulative seismic spatial distribution in the last 20 years

236 The seismic activity, apart from its spatiotemporal distribution around megathrust events (occasionally with
 237 foreshocks and normally with a hyperbolic distribution of aftershocks in time (Omori's law)), shows some



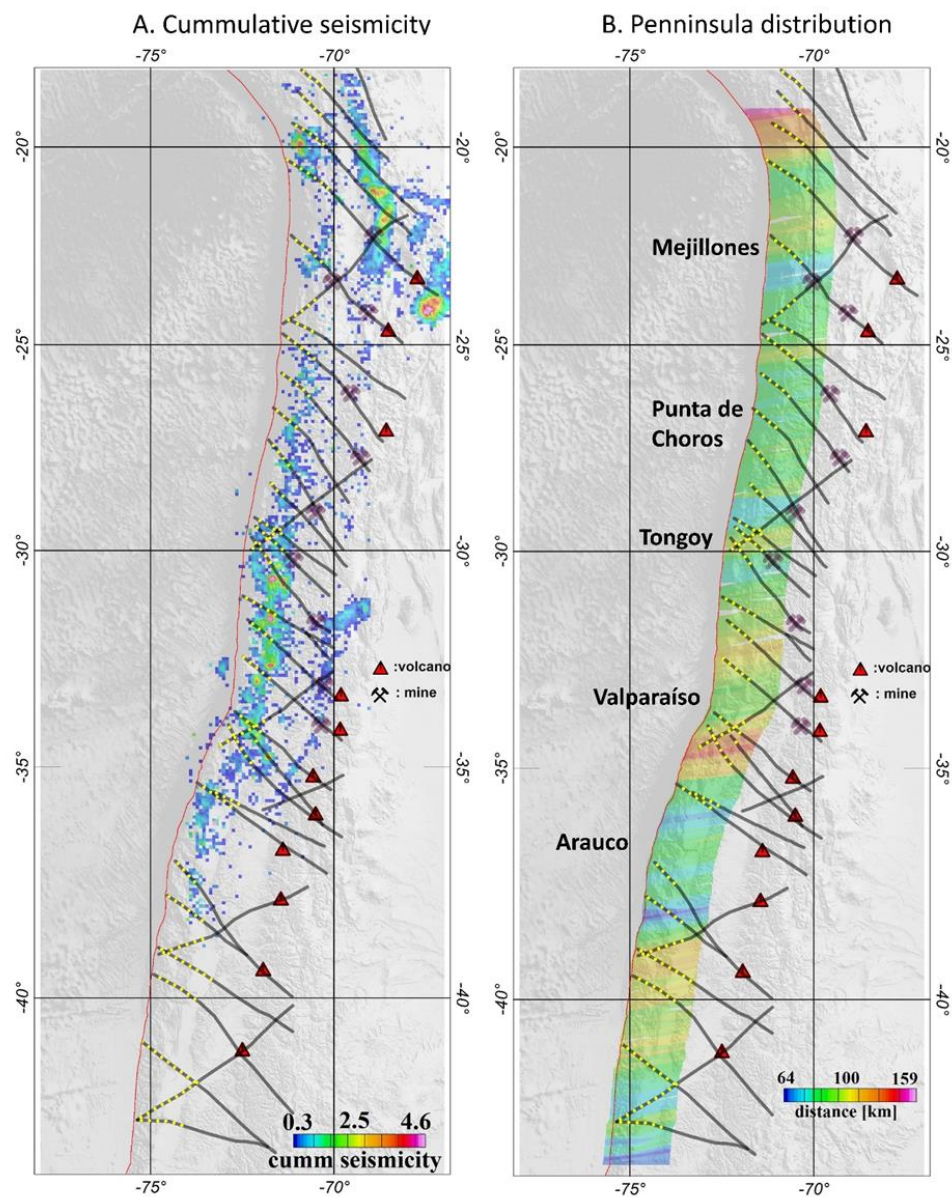
238 clustering (denominated in general as seismic swarms), that may be triggered by aseismic creep events
239 (Forsyth et al., 2003; Roland and McGuire, 2009) associated with the presence of fluids in the fault zone. In
240 the Andean plate convergence margin, recent studies also show examples of seismic swarm distribution
241 attributable to fluid pore-pressure processes (e.g. Poli et al., 2017, Pasten-Araya et al., 2018). To contextualise
242 the spatial distribution of this seismicity, we compute a normalised seismic density distribution along the
243 margin for the last 20 years in which the seismic network is complete above magnitude 3 Mw. We exclude
244 most of the seismicity associated with major thrust events in this period, filtering out the events at distances of
245 less than 200 kilometres from the rupture zone in a temporal window of 200 days. We acknowledge that this
246 20-year time window is too short to obtain a broad and complete picture of the distribution of swarms along
247 the margin. However, as swarms normally last for just a few weeks or 1–2 months at most, the cases observed
248 in this time window provide insights into their spatial distribution. The data used in this analysis were
249 obtained from the database of the National Seismological Centre (CNS in Spanish). We selected data
250 attributable to the seismogenic plate contact within a 10-kilometre-thick volume following the slab 2.0
251 Wadati-Benioff plane (Hayes 2018). The seismic density distribution is shown in Figure 3A, panel A, we can
252 see that seismicity tends to cluster in the vicinity of the seaward projection of the TLF.

253

254 **2.5 Distance from the trench to the shelf brake**

255 Saillard et al. (2016), show that peninsulas along subduction zones cost lines present a long-term permanent
256 coastal uplift that can be associated with creep and aseismic slip domains. Thus, distance from the trench to
257 the coast (DTC) constitutes a proxy to separate seismotectonic segmentation due to the weak plate coupling.
258 The physics behind this proposal lies in the dragging force that subduction force induces on the overriding
259 plate, thus with less traction (weak plate coupling in the long term), the fore-arc region close to the trench
260 should be shallower than the surroundings. To gain a broader perspective of the peninsula's distribution,
261 Figure 3B contours the distance to the shelf brake, which is probably a better proxy for a potential uplifted
262 domain in the coastal region. As shown in this figure, the DTC presents variations along the trench. We
263 identify domains of short DTC associated with peninsulas in the region near to: Arauco; Valparaíso; Tongoy;
264 Punta de Choros; and Mejillones. Based on geological and geochronological evidence in three of these
265 peninsulas (Mejillones, Tongoy, and Arauco), Saillard et al. (2016) determined uplift rates in the range of
266 0.6–2 meters per thousand years in the associated terraces. These terraces have been continuously uplifting for
267 at least the last 0.5–0.8 Myr, indicating a long-term process compared to the seismic cycle of less than 500
268 years. Using this evidence, in addition to the inter-seismic GPS coupling, Saillard et al. (2016) infer that these
269 peninsula zones are associated with weak plate coupling where deformation is mostly accommodated by
270 creep. Again, qualitatively speaking, there is a tendency to find peninsula distribution where TLF tend to
271 concentrate in the coastal region.

272



273

274

275

276

277

278

279

280

281

282

Figure 3: Panel A: density distribution of the last 20 years of seismicity in the margin; values are normalized to better define the zones where seismicity has been concentrated, filtering out all the aftershocks associated with major megathrust activity (Taltal 2001, Maule 2010, Iquique 2014, and Vallenar 2015). Panel B: distance from the trench to the shelf brake, projected to the convergence direction (10E).

2.6 Viscous coupling

The negative free-air anomaly along the Chile-Perú Trench is the response to dynamic equilibrium between buoyancy and tectonic forces (Yáñez and Cembrano, 2014). The tectonic force tends to drag the continental



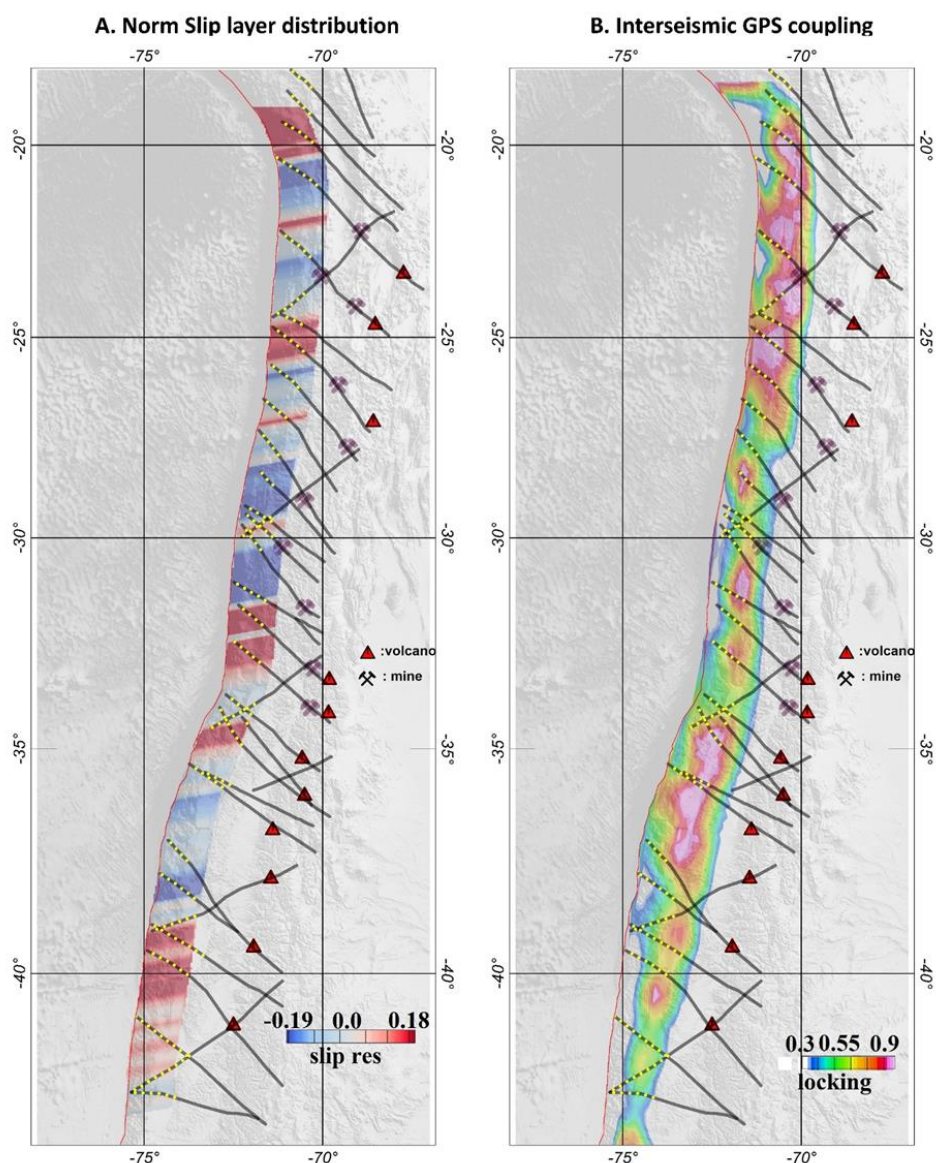
283 plate downwards, whereas buoyancy restores this deformation. Assuming equilibrium between the net
284 tectonic force and the long-term deformation (flow in continuum physics) the observed bathymetry represents
285 this force equilibrium. Therefore, for each bathymetric observation, a given Slip Layer Viscosity (SLV)
286 (Wdowinski, 1992) allows a match between observations and long-term viscous plate coupling. Using the
287 methodology developed by Yáñez and Cembrano (2004), we determine the along-strike SLV in the Nazca-
288 South America plate convergence region, considering across-strike profiles every 20 kilometres. As indicated
289 earlier, zones of maximum slip involve wavelengths larger than 20 kilometres for the megathrust events, and
290 therefore, a sample interval of 20 kilometres ensures appropriate along-strike resolution. In addition,
291 following the same rationale and conclusions of Yáñez and Cembrano (2004), we estimate that the increase of
292 the SLV in the north of the study area is due to a temperature-dependent rheology. This increase in viscous
293 plate coupling in the north is likely to be responsible for the larger crustal shortening observed in the southern
294 Andes in the last 20 Ma. Although other authors (e.g. Lamb and Davies 2003) consider that the deficiency in
295 sedimentary supply in the trench in the northern Andes is the driving mechanism for the larger viscous plate
296 coupling in the region. However, this discussion is beyond the scope of the present work, and since the
297 viscous plate coupling correctly represents the observations we are interested here in the short-wavelength
298 viscous plate response as a potential tool to identify zones with different degrees of coupling along the
299 convergent margin. Therefore, we remove this regional viscous plate coupling to isolate short-wavelength
300 features. This residual slip layer viscosity (RSLV) is included in Figure 4A (see a full discussion in
301 Supplement A). This signal shows positive (high relative viscous plate coupling) and negative (weak relative
302 coupling) zones. Again, we use normalized values to highlight the spatial distribution of the signal. In the
303 supplementary material, we present a full description of the modelling used to obtain the RSLV signal. As the
304 modelling is 1D, we extend the result of each model along the strike of the convergence (10°E).

305 **2.7 Inter-seismic GPS coupling**

306 GPS data provide information on the surface deformation relative to a stable continental reference. During the
307 inter-seismic period, the slip velocity at the intraplate contact, Vinter-seismic, can be determined from a GPS
308 network under the assumption of elastic plate deformation (e.g. Okada, 1985). This inter-seismic velocity
309 depends on the degree of plate coupling, ϕ . At maximum plate coupling ($\phi=1$), Vinter-seismic is null, and at
310 minimum plate coupling ($\phi=0$), Vinter-seismic is equal to the convergence velocity ($V_{convergence}$) (e.g.
311 Nuvel1a, De Mets, et al., 1994). Or, mathematically (e.g. Metois et al., 2012), $V_{inter-seismic}=(1-\phi)*$
312 $V_{convergence}$. Inter-seismic GPS coupling is presented as GPS locking data in Panel B of Figure 4 (based in
313 a compilation of GPS information derived from different sources, Burgmann et al., 2005; Chlieh et al., 2008;
314 Loveless & Meade, 2011; McCaffrey et al., 2002; Metois et al., 2012, 2016; Moreno et al., 2010, 2012;
315 Wallace et al., 2004)). From 27°S to the north, high GPS plate coupling is generally observed, although some
316 correspondence is observed with the local minimum and TLF distribution. Between 27°–33°S, the GPS
317 coupling shows domains with lower values with better correspondence with TLF segmentation and the
318 minimum in viscous coupling. To the south of 33°S, the GPS plate coupling shows a spatial distribution that
319 again shows some coincidence with the other proxies, but also some discrepancies. This is not surprising,
320 since GPS inter-seismic plate coupling reflects the quasi-instantaneous coupling of seismo-tectonic segments



321 at different loading stages. Nevertheless, in most of the studied segments, the GPS plate coupling correlates
322 relatively well with the viscous plate coupling, and the location of peninsulas and cumulative seismicity in the
323 last 20 years.
324



325
326 **Figure 4: Panel A: Normalized Residual slip layer viscosity (RSLV) derived from 1D modelling along profiles**
327 **separated every 10 km and oriented along the Nazca-South American plate convergence (10°N); as this model**
328 **involves all of the slip layer, its spatial distribution is represented from the trench until 150 km landward. Panel B:**
329 **GPS inter-seismic plate coupling, model 2017 (Burgmann et al., 2005; Chlieh et al., 2008; Loveless & Meade, 2011;**
330 **McCaffrey et al., 2002; Metois et al., 2012, 2016; Moreno et al., 2010, 2012; Wallace et al., 2004).**



331 **3. Discussion**

332 **3.1 Quantitative correlation between TLF and plate coupling proxies derived from seismicity**
333 **distribution, GPS and viscous coupling and coastal morphology.**

334 In order to better quantify the correspondence between the spatial distribution of TLF and the indirect estimate
335 of plate coupling described in chapter 3 we present here an objective comparison between them. This task is
336 challenging, taking into consideration the poorly constrained data used: (a) in some cases, regional-scale
337 geological observations (TLF and peninsula distribution); (b) different time-scale coupling estimates (inter
338 seismic GPS locking and long term viscous coupling); (c) poorly resolved GPS solution offshore; (d) 1D
339 modelling of viscous coupling; and (e) The lack of completeness in the seismicity record (historical record of
340 500 years, instrumental record of megathrust events of 50 years, and cumulative seismicity of 20 years)
341 considering a seismic cycle of a couple of hundred years in the margin. Thus, none independent proxy is capable
342 to produce a reliable estimate by itself, but rather a combination of them. Therefore, a thorough analysis is
343 beyond the capabilities of the data source, and what we present here, though quantitative, should be understood
344 as a guide to determine tendencies from different and independent perspectives that as a whole, provide a more
345 robust estimate on the link between TLF and plate coupling in the margin.

346 The approach adopted considered the spatial correlation between TLF and the six proxies described in chapter
347 3, using the Pearson correlation coefficient between two variables (r_{xy}) defined as:

348

$$349 \quad r_{xy} = \frac{\sum_{i=1}^n (x_i - \bar{x})(y_i - \bar{y})}{\sqrt{\sum_{i=1}^n (x_i - \bar{x})^2 \sum_{i=1}^n (y_i - \bar{y})^2}} \quad (1)$$

350 Where \bar{x} and \bar{y} are the average value of each variable. This function r_{xy} has values between -1 (opposite
351 correlation) to 1 (direct correlation). Values near zero mean weak or null correlation. In the application of the
352 Pearson correlation in this case, the spatial distribution of TLF is always the x_i , and the 6 proxies used in this
353 case are the y_i in each case. A key property of the Pearson correlation coefficient is its invariance to spatial
354 distribution of samples and scale of the two variables. This property is particularly useful in this case where we
355 are trying to correlate very different proxies in terms of spatial distribution and scale. The correlation is
356 performed in moving windows bins of 32x32 km², with an overlap of 50% between correlation estimate. The
357 correlation is calculated in a domain of 140 km width from the trench to the east, the plate coupling zone where
358 short-term and long-term processes take place.

359 TLF are defined as line traces, but in order to spatially correlate them with the other variables, we add
360 a width, considering potential spatial uncertainties and zones of influence. Thus, the width of each TLF is treated
361 as a gaussian with a value of 1 in the centre and 0 at the edge, located at 10 km from the centre, representing
362 the deformation zone and the lateral surface covered by the potential fluid release. Such a width of 20 km seems
363 a reasonable number for a fault system of more than 100km length (>20%). In fact, in recorded earthquakes,
364 like the Landers earthquake 1992 (Mw 7.3) where a rupture length of 85 km has been determined, with a shear
365 deformation zone of 12-16 km (Perrin et al., 2020). Outside the TLF domains a value of -1 indicate no spatial
366 distribution of TLF, but in practice is not relevant because the correlation is focussed inside the TLF domain



367 only. The other six proxies are treated in different manner, depending on its nature. GPS plate coupling is a
368 spatial variable covering the whole spatial range of the coupling. Looking at the GPS coupling described in
369 Figure 4b, we can see that most of the plate contact is highly coupled, well above 0.6 almost everywhere, thus
370 in order to identify some differences in coupling we setup the mean value at 0.8. Slip viscosity layer and distance
371 from the shelf brake to the trench are single values varying with latitude which are extended to spatial variables
372 projecting the value landward following the convergence direction ($\sim 10^\circ\text{E}$). In the case of the slip coupling a
373 mean value is already removed, thus a mean value of 0 is considered. For the shelf brake-trench distance we
374 use the average separation of 100km as the mean value. Seismic cumulative density and slip distribution of
375 megathrust events define restrictive domains along the plate coupling region. These areas are normalized
376 between 1 and zero, and outside the region a value of -1 is assigned (no data). The same procedure is used for
377 the boundary between historic seismicity segmentation, value 1 in the transition, and -1 outside. Since the
378 analysis is restricted to the correlation between TLF's and the six proxies, the correlation only concerns the
379 inner part of the TLF. Given the nature of each proxy, a low coupling at a given TLF implies a negative Pearson
380 correlation at GPS and viscous coupling, distance from the shelf brake to the trench, and slip distribution for
381 megathrust events (maximum slip should lie outside the TLF domain). On the contrary, positive Pearson
382 correlation is expected with the historic segmentation and cumulative seismicity, to reflect low coupling at the
383 TLF domain.

384 The results for each Pearson correlation coefficient spatial distribution are presented in Figure 5 in a
385 plan view. In Figure 6 we present the result for the 32 relevant TLF in terms of the histogram obtained for the
386 Pearson correlation inside the corresponding TLF domain. Over the histograms observations we include an
387 interpretation on the correspondence with a low plate coupling condition, depending on the shape of the
388 histogram, positive (Pearson correlation biased to the left in GPS, VISC, DIST, SLIP histograms; and biased to
389 the right in the CUMM and HIS histograms), unclear (flat for all the proxies) and negative (Pearson correlation
390 biased to the right in GPS, VISC, DIST, SLIP histograms; and biased to the left in the CUMM and HIS
391 histograms) correlation. Based on this analysis we qualify the potential of each TLF in terms of its barrier
392 potential, high, ambiguous, and poor. The criteria to establish this qualification considers the following: (a) high
393 potential: at most one correlation is negative and by majority are positive correlation; (b) ambiguous: at most
394 two correlations are negative and at least one correlation is positive; (c) poor: when more than three correlations
395 are negative or none of them are positive.

396 Some relevant conclusions arise from the spatial analysis of Figure 5 and histograms of Figure 6:

- 397 1. From the 32 relevant TLF in terms of plate coupling, 63% (20 of 32) show a high potential for a
398 barrier behaviour, 31% (10 of 32) presents some ambiguity, and only 6% (2 of 32) TLF show a poor
399 chance to become a barrier domain.
- 400 2. For the case of ambiguous potential, almost all of them present at least 2 positive correlation proxies.
- 401 3. For individual histograms, 54% histograms show a positive correlation, 28% are considered
402 ambiguous, and 18% present a negative correlation.

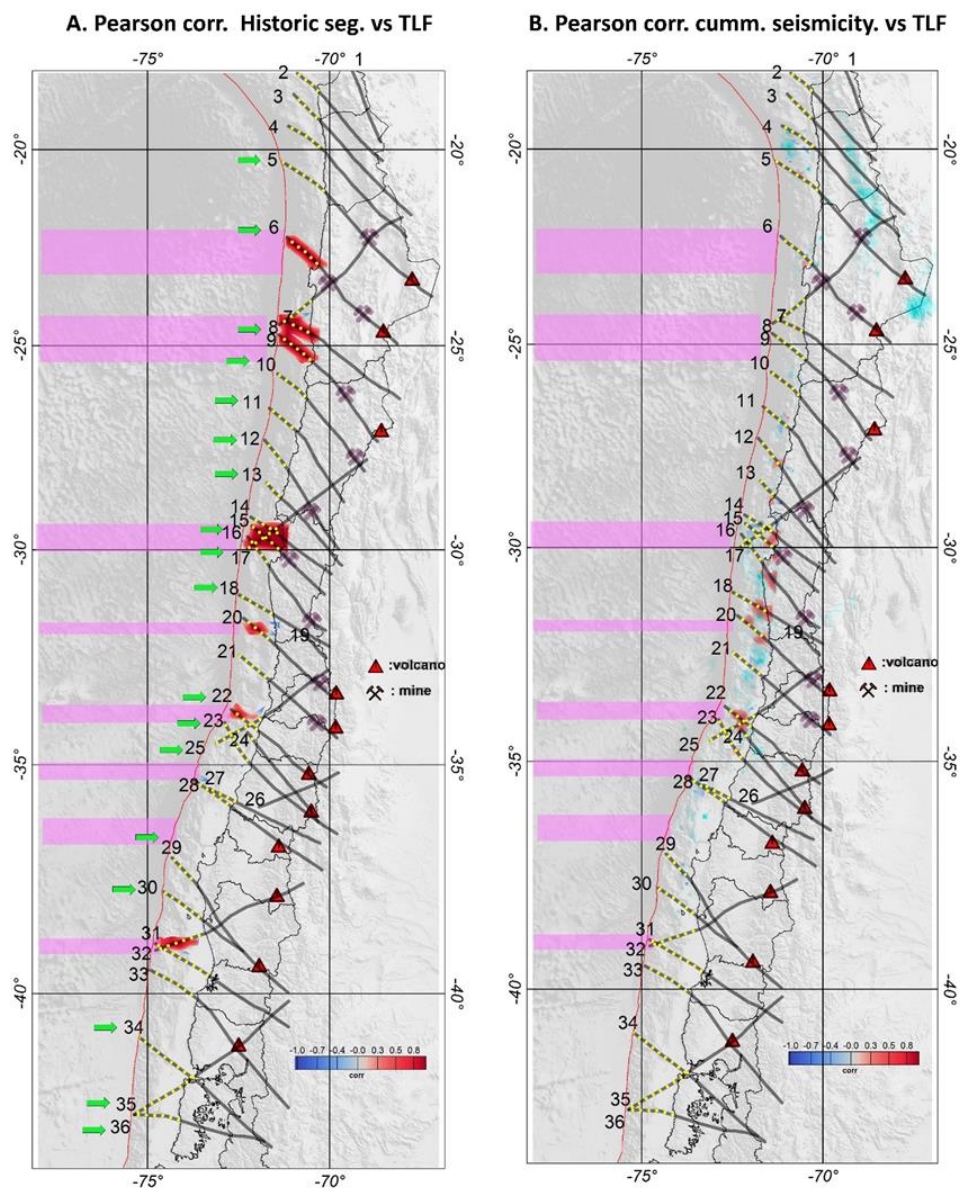


- 403 4. Five out of seven seismotectonic boundary segments present a strong correlation with TLF spatial
404 distribution (Figure 5a). In terms of particular histogram distribution, 11 out of 13 show a positive
405 correlation and none of them show a negative correlation.
- 406 5. The cumulative interseismic seismicity (Figure 5a), perhaps the weakest proxy due to the lack of
407 seismic completeness due to the very restricted time window of observation, still shows an almost
408 100% direct correlation with the TLF traces where inter-seismic activity developed (TLF 14-15-16,
409 TLF 18-20, TLF 22). In terms of the histogram distribution, shows a rather similar pattern, some
410 clear positive correlation in 6 out 18 TLF and a none conclusive solution in 12 out 18 cases.
- 411 6. The spatial distribution of the slip zones of the main megathrust events recorded in the last 50 years,
412 show a minimum positive correlation with the spatial distribution of TLF. As we can see in Figure
413 5b, less than 20% of the total slip domains, potential zones of asperities, correlate positively with
414 TLF. The remaining 80% lies outside the zone of influence of TLF. In the histogram distribution,
415 the same pattern is observed, 57% of negative Pearson correlation (or positive correlation in terms
416 of low plate coupling), 26% of ambiguous solution and 17% positive Pearson correlation. It is
417 important to note that in several histograms of this proxy a positive correlation is adopted when a
418 low flat response is observed, but in the left side there is a single column saturated at the maximum
419 value for correlation -1 (most of the TLF is empty, or in other words the slip zone lies outside the
420 TLF domain).
- 421 7. In the GPS plate coupling-TLF Pearson correlation coefficient (Figure 5b) 50% of the cases show a
422 negative correlation (low relative coupling), whereas 30% show some mix results, with the negative
423 correlation concentrated in the deeper parts of the coupling, and only in 20% of the cases a positive
424 correlation holds, mostly concentrated in the coupling zone of the Antofagasta 1995 and Tocopilla
425 2007 earthquakes, and probably linked with some post seismic effects. Consistently, in 18 out of 32
426 (56%) histograms responses (Figure 6), the low coupling correlation is observed, whereas in 10 out
427 of 32 (31%) the response is ambiguous, and the remaining 13% is associated with relatively high
428 GPS coupling. We acknowledge that these values are very much conditioned by the choice of the
429 threshold of 80% to separate high to low GPS coupling, but the aim is to identify less coupled
430 domains in a signal almost saturated with high values.
- 431 8. The same type of analysis was performed for the Slip Layer viscosity – TLF Pearson correlation
432 coefficient (Figure 5c). In 50% of the case the correlation is opposite (low viscosity slip zones
433 corresponds with the location of TLF). In 15% of the cases, we observed mixed results, whereas in
434 35% of the cases the correspondence is positive. Similar results are obtained with histogram
435 responses (Figure 6), in 17 out of 32 (53%) the low coupling correlation is observed, whereas in 6
436 out of 32 (19%) the response is ambiguous, and the remaining 28% is associated with relative high
437 slip viscosity. One important limitation of this approach is the 1D approximation of an inherently
438 3D process. This fact is probably the main reason for its relatively low positive response compared



439 to the other proxies. Finally, figure 5c show the Pearson correlation coefficient for the distance from
440 the shelf brake to the trench. In this case, the closest shelf brake to the trench at TLF intersection is
441 a 36%, the same number of cases show an opposite behaviour and only 28% presenting mixed
442 results. In terms of the histogram distribution (Figure 6), the same tendency is observed, but with a
443 higher predominance of shorter distance shelf brake-trench (44%), whereas the opposite is observed
444 in 34% of the cases and 22% show an ambiguous response. This is the proxy that show the lowest
445 level of positiveness, probably due to the fact that other processes are also involved in the uplift of
446 the peninsula regions, for instance the density of the crust and its relative buoyancy.

447 As we point out earlier in the text, none of the proxies by itself have the merit to account for the degree of
448 coupling along the subduction zone, and the results emanated from the Pearson correlation demonstrate that.
449 However, when we integrated the individual results 63% of the TLF can potentially behave as barrier, and only
450 in two cases (6%) chances are poor. In the remaining 31% of the cases, represented as ambiguous cases, there
451 are still some evidences of positive correlations in more than one proxy. In Figure 5a, panel A, we include a
452 reference for the TLF with high potential to become a barrier (green arrow), and we can see that in almost all
453 the cases they are consistent with the tectonic segmentation derived from the historic seismicity. One peculiar
454 distribution of potentially active barrier domains is observed between 25°-30° S, the zone with less historical
455 seismicity (Figure 2). On the other hand, not necessarily all the TLF behave as barriers, due to lack of favourable
456 orientation, depth extent, age, dip angle, fluid content among other uncertainties. Therefore, we consider that
457 the previous semiquantitative analysis including all the proxies, support the presence of a geological signal of
458 low plate coupling when TLF is present. In the next section we propose a conceptual mechanism to explain
459 this phenomenon.
460



461

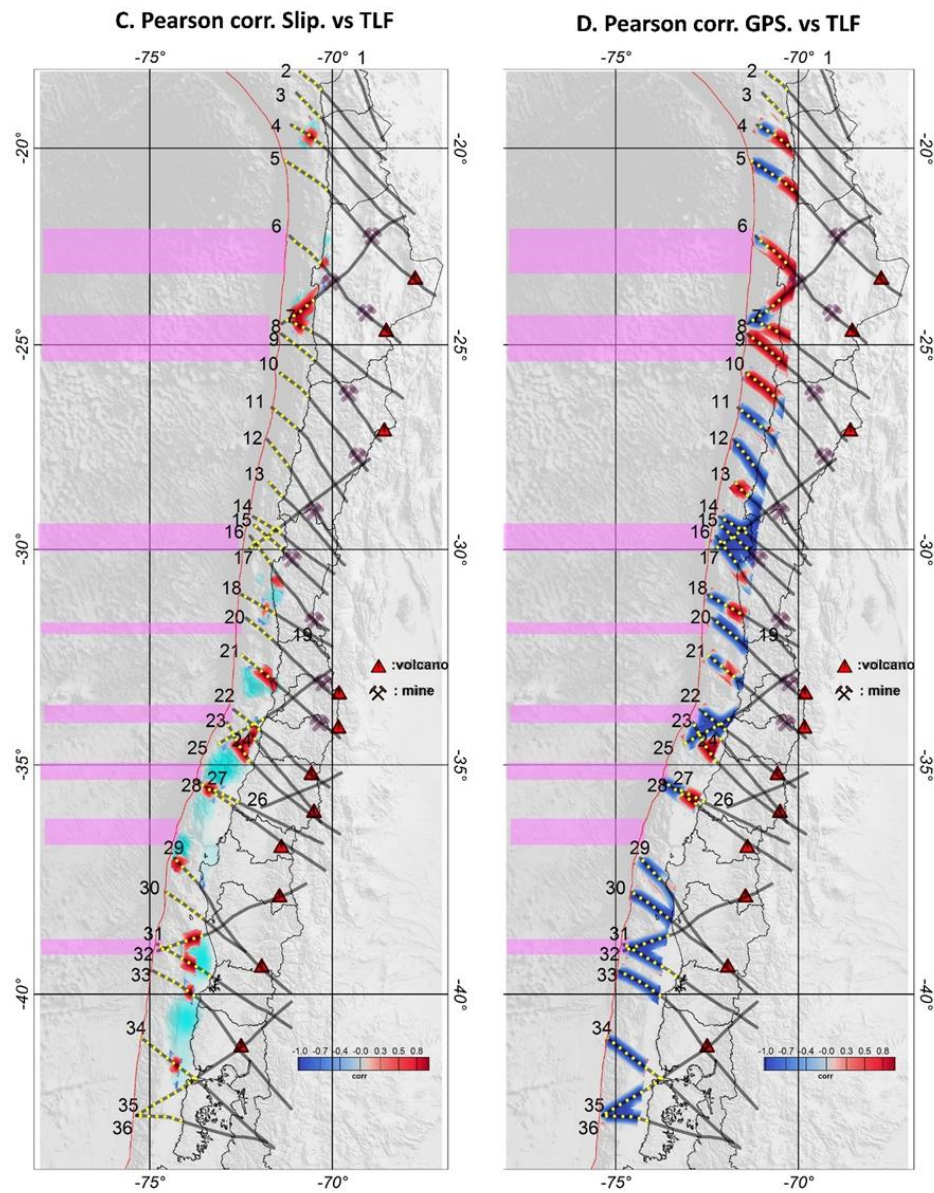
462

463

464

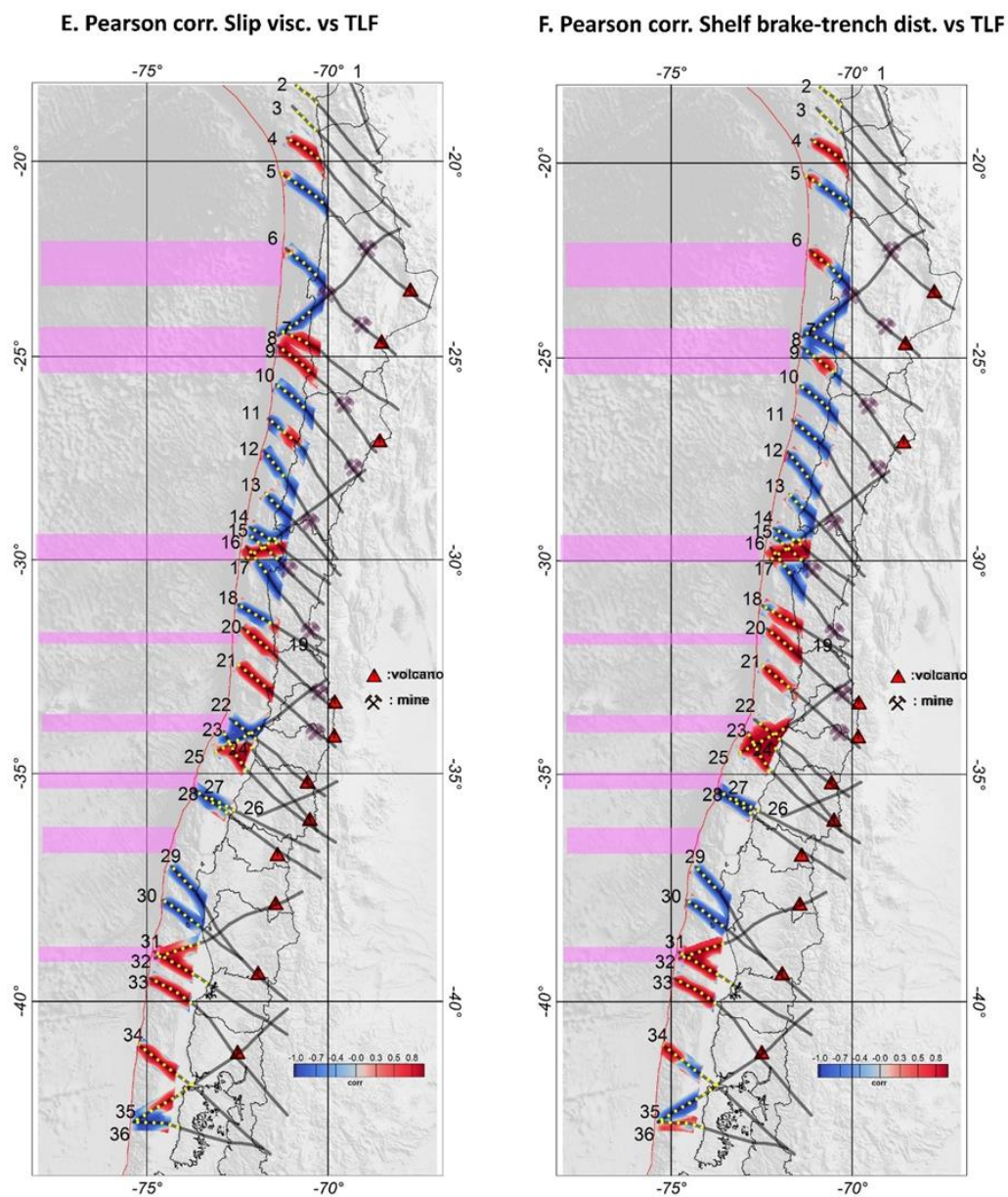
465

Figure 5a: Pearson correlation coefficient between TLF and (A) tectonic segmentation and (B) cumulative seismicity. Colour code range from -1 (opposite correlation) to 1 (direct correlation). In panel A the green arrow shows the TLF with high potential as a barrier, according with the criteria established from histograms distribution of Figure 6.



466
467
468
469
470

Figure 5b: Pearson correlation coefficient between TLF and (c) normalized slip viscosity and (d) GPS coupling. Colour code range from -1 (opposite correlation) to 1 (direct correlation).



471

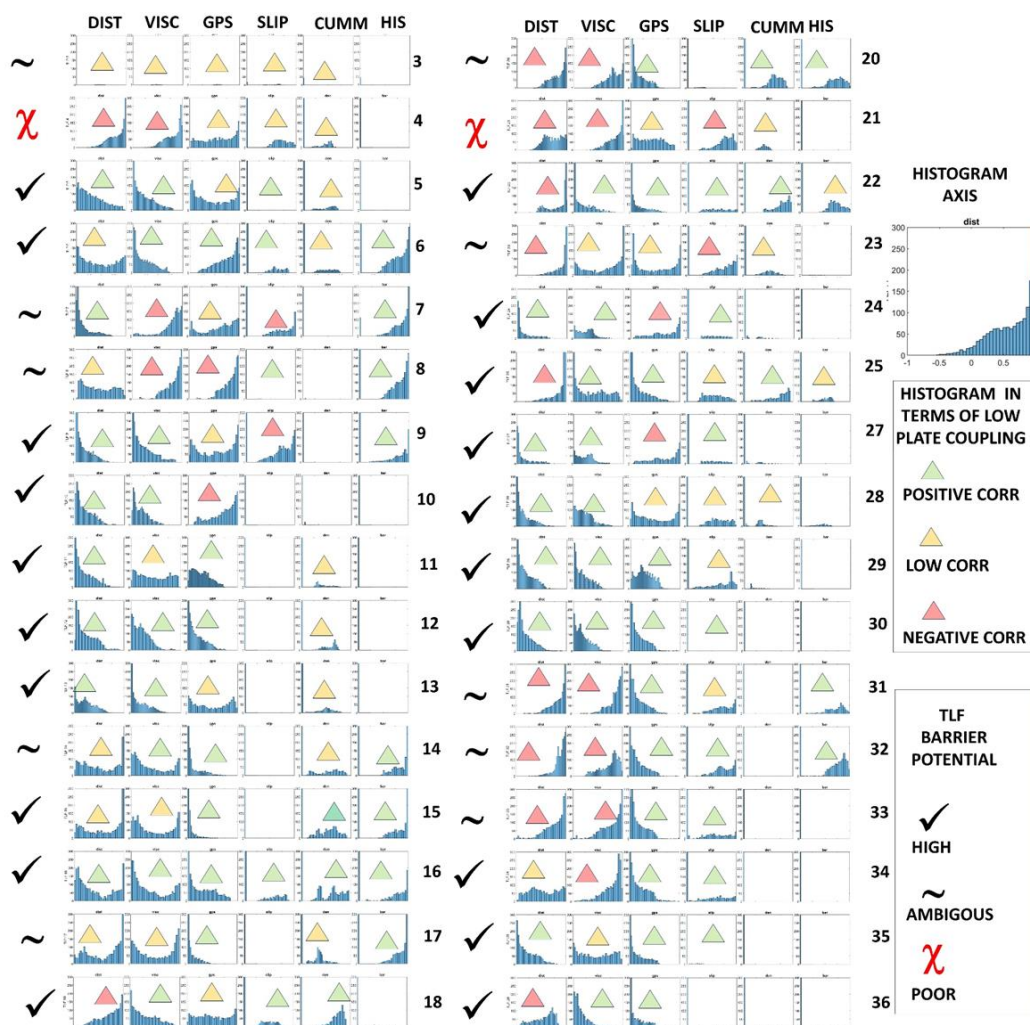
472

473 **Figure 5c: Pearson correlation coefficient between TLF and tectonic slip viscosity (e), and distance from the trench**

474 **to the shelf brake (f). Colour code range from -1 (opposite correlation) to 1 (direct correlation).**

475

476



477
478
479
480
481
482

Figure 6: Histogram diagrams for Pearson correlation in each TLF. Histogram interpretation and TLF qualification as a potential barrier is indicated in inlet. TLF number is indicated to the left of each panel (a good resolution of this image is provided in the supplementary material).



483 **3.2 A simple conceptual barrier model: misoriented TLF as a store/released of fluids during the seismic**
484 **cycle.**

485 Comparing the spatial distribution of the seaward extension of the TLF and the previously discussed first-order
486 conditioning factors of the tectonic segmentation in the Andes (chapter 2), and the cross correlation described
487 in section 4.1, we can make the following conclusions:

- 488 1. The coastal termination of an TLF generally occurs close to a peninsula, where the shortest trench–
489 coast distance is observed, in spatial correspondence with zones of negative RSLV (weak viscous
490 coupling), and in some cases also corresponding to zones of weak GPS coupling. However, it should
491 be noted that the degrees of coupling inferred via RSLV and GPS do not map similar observation
492 time windows, covering geological (Ma) vs seismic cycle (300–500 years) time frames, respectively.
- 493 2. During the last 60 years, slip displacements during the major megathrust earthquakes in the margin
494 of Chile tend to be bounded by the coastal termination of an TLF in their northern and southern
495 boundaries. Thus, if these slip zones represent a spatial distribution of asperities, the TLF correspond
496 to zones potentially associated with barriers, consistent with the long-term low coupling inferred
497 from RLSV, GPS plate coupling and distributions of peninsulas. the previous long-term
498 observations.
- 499 3. Cumulative seismic activity in the last 20 years tends to nucleate in the vicinity of the seaward
500 termination of the TLF, normally with the development of seismic swarms of 100–300 events of
501 medium to low magnitudes during periods of several weeks at most.
- 502 4. The geological record demonstrates that TLF are long-lived structures of high permeability in
503 comparison with the surrounding crust and most likely the underlying mantle as well, and are thus
504 potentially efficient fluid storage structures.

505 The previous observations provide the grounds to propose a simple conceptual model to understand the role
506 played by TLF in the tectonic segmentation of a convergent margin. These observations consistently show that
507 TLF in the seismogenic zone are spatially correlated with long-term and short-term evidence of weak coupling
508 behaviour. The long-term evidence involves geological processes that build up during many seismic cycles,
509 over a time frame of millions of years, including low values of slip-layer viscosities and correspondence with
510 the spatial distribution of peninsulas. The short-term evidence involves fragments of the seismic cycle over a
511 time frame of less than 500 years, characterized by weak coupling zones as inferred by inter-seismic GPS
512 observations, the flanks of slip zones of recent mega-thrust events, and the boundaries that delimit the historical
513 record of major events. Overall, these observations consistently show that TLF domains are likely candidates
514 for barrier zones.

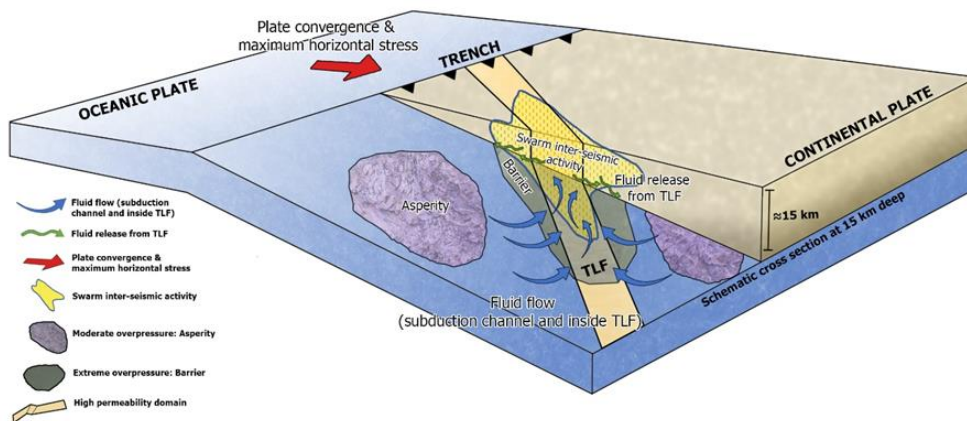
515 From basic principles, the strength of a fault is controlled by the friction at the discontinuity plane. According
516 to Amonton's law, the fault strength is proportional to the product of the normal stress and the static or dynamic
517 friction (e.g. Scholz, 1990). In the presence of fluids, pore pressure reduces the normal stress, thereby reducing
518 the strength of the fault (e.g. Scholz, 1990), eventually to zero if the pore pressure reaches the lithostatic pore



519 pressure. Under these supra-lithostatic fluid pressure conditions, even faults that are strongly misoriented for
520 frictional reactivation under the prevailing stress field can be reactivated, focusing the discharge of large
521 amounts of overpressured fluids and acting as a “fault-valve” (Sibson, 1990; Cox, 2016). Indeed, Cox (2016)
522 showed that, under supra-lithostatic fluid pressure conditions, the typical seismic response in the faults
523 corresponds to microseismic swarms, which, according to Sibson (2020), would concentrate at the roots of the
524 fault system. In the case of an TLF, which is a long-lived structure transecting the whole lithosphere (e.g., Lutz
525 et al., 2022), the root of the fault system at the Andean convergent margin corresponds to the subduction
526 channel. Low fault strength at subduction zones can be equated to barrier zones where convergence is mostly
527 accommodated by creep and/or micro-seismicity. The hydration of the subducting slab during its bending in the
528 outer rise region has been widely documented in different subduction margins (e.g., Holbrook et al., 1999;
529 Shillington et al., 2015; Contreras-Reyes et al., 2007; Moscoso and Grevemeyer, 2015; Ranero and
530 Sallarès, 2004; Fujie et al., 2018, among others), as has the slab’s subsequent dehydration during subduction
531 (Barriga et al., 1992; Maekawa et al., 1993; Peacock, 1993). Mantle hydrous phases (serpentinites) have also
532 been observed in forearc regions at subduction margins (e.g. Hyndman and Peacock, 2003; Xia et al., 2015;
533 Hansen et al., 2016), further demonstrating that subduction systems transport large amounts of water; however,
534 the amount of water transported is still unknown (Miller et al. 2022). On the other hand, fluid flow in porous
535 media is governed by Darcy’s law, in the opposite direction to the hydraulic head and proportional to the
536 hydraulic permeability. Numerical models (Menant et al., 2019) have been used to determine the path of
537 overpressured fluid flow along the subduction channel, and how strong/weak frictional channels condition the
538 flow (weak frictional channel zones percolate more water upwards compared to strong frictional channel zones).
539 These two domains determine the location of weak and strong coupling zones at the plate contact. Thus,
540 according to basic principles and numerical models, water concentrates in zones of high permeability.
541 The geological record on land shows that, in the Andean margin, TLF are associated with ore deposits
542 clustered at the intersection of magmatic arcs that become progressively younger eastward (Piquer et al.,
543 2016; Yáñez and Rivera, 2019; Piquer et al., 2021a; Farrar et al., 2023; Wiemer et al., 2023), covering the full
544 tectono-magmatic history during the Mesozoic and Cenozoic. Local seismic networks deployed in Northern
545 and Central Chile also show alignments of seismic activity along some TLF systems (Yáñez and Rivera,
546 2019; Piquer et al., 2019, 2021a; Sielfeld et al, 2019; Pearce et al., 2021). These long- and short-term
547 observations indicate the presence of long-lived high-permeability domains along the TLF systems in the
548 Andean margin of Northern and Central Chile. Therefore, we postulate that TLF act as fluid sinks in the
549 forearc region, following a continental-scale fault-valve behaviour, carrying the fluids released by slab
550 dehydration and transported from distal locations through the subduction channel and discharging the fluids
551 upwards and laterally through the TLF. Thus, if the proposed mechanism operates for long periods of time,
552 the fluid distribution at the plate contact should show an uneven distribution of fluid, delimitating domains of
553 weak and strong friction channels, which would act as seismic barriers and asperities, respectively. In this
554 context, the spatial distribution of TLF would be associated with barriers that delimitate the tectonic
555 segmentation. In the proposed model, tremor or swarm seismic activity represent episodic fluid release from
556 TLF that are poorly oriented with respect to the regional tectonic stress — in this case, the NW-striking fault



557 systems oriented at a high angle relative to the ENE convergence direction. This model provides a causal link
558 between the presence of TLF in the upper plate and the distribution of barrier and asperity domains in the
559 plate interface. A schematic cartoon of this model is presented in Figure 7.
560 .



561
562 **Figure 7: Schematic conceptual model of fluid transport towards TLF, following different paths in the subduction**
563 **channel, as well as upwards within the TLF. This model proposes that TLF are sink domains of slab-derived fluids**
564 **that promote the development of barrier zones and dry out the neighbouring domains where asperities develop.**
565 **Swarm clustering in spatial association with the TLF represents a mechanism for the quasi-creep release of energy**
566 **within the barrier zone.**

567
568 **3.3 Implications**

569 If TLF act as low-friction domains (barriers) due to their capacity to store fluids released from the subducting
570 slab and thereby dry out neighbouring zones of the subduction channel, promoting the development of a high-
571 friction domain (asperity), we can envision a series of implications derived from the proposed model.

572 The most relevant implication is the geological control of barrier zones. This geological control exerted by high-
573 permeability domains in the continental lithosphere (TLF) implies a spatial control of barrier zones, and thus
574 the seismotectonic segmentation should be stable for several seismic cycles as long as the capacity of TLF to
575 store fluids is maintained. If this scenario is correct, the estimate of the seismic risk associated with each
576 seismotectonic segment can be assessed based on empirical fault-length laws (e.g. Anderson et al., 2016). In
577 this context, interplate seismic swarms and slow seismic events that develop in the vicinity of TLF zones would
578 be a mechanism for the steady release of seismic energy.

579 As discussed previously, several TLF have been identified in the Andean margin; however, little is known about
580 their origin, width, dip, depth extent, and capacity to behave as a water sink. Therefore, further study is needed
581 to postulate a reliable map of barrier domains in this subduction system.



582 On the other hand, seismic barriers/asperities would be conditioned by the capacity of barrier zones to
583 mobilise and store fluids, and would thus be relatively stable in space but with a variable behaviour during
584 several seismic cycles. If the age of the subducted slab conditions the water budget at the plate interface
585 (Rupke et al., 2004), the progressive age increase from south to north in this margin (from 0 to 45 Ma) would
586 be a controlling factor for the efficiency of the TLF-barrier hypothesis. Although this implication is highly
587 speculative, the historical record shows that the largest megathrust events at the margin have occurred in
588 Southern Chile, including the 9.3Mw 1960 Valdivia Earthquake, the largest event recorded worldwide.

589

590 4. Conclusions

591 Based on first order geological and geophysical observations of the Nazca-South America plate convergence
592 we propose a conceptual model to understand the tectonic segmentation in the Andean region.

593 Observations include historical seismicity and the associated seismotectonic segmentation. Major thrust events
594 occurred in the region in the last 60 years, defining domains of asperities. GPS and viscous plate coupling that
595 provide independent proxies to establish potential domains of barriers (low plate coupling) and asperities (high
596 plate coupling). Location of low plate coupling domains is further associated with the spatial distribution of
597 peninsulas (less basal erosion) and cumulative seismicity during the inter-seismic period (slow interplate
598 seismic events, creeping, associated with fluid release).

599 Key element in the model is played by trans-lithospheric faults (TLF). Landward, this TLF system concentrate
600 the occurrence of major hydrothermal ore deposits and some active volcanism, denoting their intrinsic high
601 permeability. Thus, at their seaward edge the TLF domains act as sink and release of fluids during the seismic
602 cycle. The fluid is captured from the slab through the subducting channel, and continuously release to the plate
603 contact, promoting the growth of barriers beneath them (excess of fluids), and asperities laterally (reduction in
604 fluid content).

605 If the interaction of first order continental structures and the fluid content of the subducting slab plays a
606 central role in the seismotectonic segmentation of convergence zones, a carefully understanding of the
607 overriding plate geology and associated structures could be instrumental to better understand the associated
608 seismic risk.

609

610 **Competing interests:** The contact author has declared that none of the authors has any competing interests.

611 **Acknowledge:** This research was partially supported by Fondef project D10I1027. J.P. acknowledges support
612 from ANID-FONDECYT grant 11181048 and Amira Global P1249 project.

613 **Data Availability Statement:** The data used in this paper is derived from published papers, indicated in the
614 text, and topographic/bathymetric data extracted from public source, ETOPO 2022. DOI: 10.25921/fd45-gt74.



References

- Aki, K., (1984). Asperities, barriers, characteristic earthquakes and strong motion prediction. *Journal of Geophysical Research* 89: doi: 10.1029/JB089iB07p05867. Issn: 0148-0227.
- Angermann, D., J. Klotz, C. Reigber, (1999). Space-geodetic estimation of the Nazca–South America Euler vector. *Earth and Planetary Science Letters*, 171(3), 329–334. [https://doi.org/10.1016/S0012-821X\(99\)00173-9](https://doi.org/10.1016/S0012-821X(99)00173-9).
- Arriagada, C., P. Roperch, C. Mpodozis, G. Dupont-Nivet, P.R. Cobbold, A. Chauvin, J. Cortés, (2003). Paleogene clockwise tectonic rotations in the forearc of central Andes, Antofagasta region, northern Chile. *Journal of Geophysical Research: Solid Earth*, 108(B1).
- Aron, F., R. Allmendinger, J. Cembrano, G. González, and G. Yáñez, (2013). Permanent Forearc Extension and Seismic Segmentation: Insights from the 2010 Maule Earthquake, Chile, *J. Geophys. Res.*,doi:10.1029/2012JB009339,
- Avouac, J.P., (2007). Dynamic Processes in Extensional and Compressional Settings - Mountain Building: From Earthquakes to Geological Deformation, *Treatise on Geophysics*, 6 , 377 – 439.
- Barrientos S.E. , S. N. Ward, (1990). The 1960 Chile earthquake: inversion for slip distribution from surface deformation, *Geophysical Journal International*, Volume 103, Issue 3, Pages 589–598, <https://doi.org/10.1111/j.1365-246X.1990.tb05673.x>.
- Barriga F. J. A. S., W.S. Fyfe, L.A. LANDEFELD, A. Ribeiro, (1992). Mantle exhumation: Tectonic fluidisation at depth. *Earth Science Reviews* 32, 123-9.
- Bilek, S. L., S.Y. Schwartz, H.R. DeShon, (2003). Control of seafloor roughness on earthquake rupture behavior. *Geology* 31, 455–458
- W. F. Brace, J. D. Byerlee ,Stick-Slip as a Mechanism for Earthquakes.*Science*153,990-992(1966).DOI:10.1126/science.153.3739.990
- R. Burridge, L. Knopoff; Model and theoretical seismicity. *Bulletin of the Seismological Society of America* 1967; 57 (3): 341–371. doi: <https://doi.org/10.1785/BSSA0570030341>Bürgmann, R., Kogan, M. G., Steblov, G. M., Hilley, G., Levin, V. E., & Apel, E. (2005). Interseismic coupling and asperity distribution along the Kamchatka subduction zone. *Journal of Geophysical Research*, 110, B07405. <https://doi.org/10.1029/2005JB003648>
- Cahill T. and B.L. Isacks, (1992). Seismicity and shape of the subducted Nazca Plate, *Journal of Geophysical Research*, vol 97, B12, 17503-17529.
- Carretier, S., Regard, V., Vassallo, R., Aguilar, G., Martinod, J., Riquelme, R., ... & Lagane, C. (2013). Slope and climate variability control of erosion in the Andes of central Chile. *Geology*, 41(2), 195-198.
- Cembrano J., and L. Lara, (2009). The link between volcanism and tectonics in the southern volcanic zone of the Chilean Andes: A review, *Tectonophysics* 471, 96–113.



- Chernicoff, C.J., J.P. Richards, E.O. Zappettini, (2002). Crustal lineament control on magmatism and mineralization in northwestern Argentina: geological, geophysical, and remote sensing evidence. *Ore Geology Reviews* 21, 127-155.
- Chlieh M., J. B. De Chabaliér, J. C. Ruegg, R. Armijo, R. Dmowska, J. Campos, K. L. Feigl, (2004). Crustal deformation and fault slip during the seismic cycle in the North Chile subduction zone, from GPS and InSAR observations, *Geophysical Journal International* Volume 158, Issue 2 p. 695-711.
- Chlieh, M., Avouac, J. P., Sieh, K., Natawidjaja, D. H., & Galetzka, J. (2008). Heterogeneous coupling of the Sumatran megathrust constrained by geodetic and paleogeodetic measurements. *Journal of Geophysical Research*, **113**, B05305. <https://doi.org/10.1029/2007JB004981>
- Comte D., A. Eisenberg, E. Lorca, M. Pardo, L. Ponce, R. Saragoni, S. K. Singh, G. Suárez, (1986). The 1985 Central Chile Earthquake: A Repeat of Previous Great Earthquakes in the Region?, *Science*, 07-25 233(4762): 449-453.
- Contreras-Reyes, E., I. Grevemeyer, E. R. Flueh, M. Scherwath, and M. Heesemann, (2007). Alteration of the subducting oceanic lithosphere at the southern central Chile trench–outer rise, *Geochem. Geophys. Geosyst.*, 8, Q07003, doi:10.1029/2007GC001632.
- Cox, S.F., (2016). Injection-driven swarm seismicity and permeability enhancement: implications for the dynamics of hydrothermal ore systems in high fluid-flux, overpressured faulting regimes. *Economic Geology* 111, pp. 559–587.
- Creixell, C., Parada, M. A., Morata, D., Vásquez, P., Pérez de Arce, C., Arriagada, C., (2011). Middle-Late Jurassic to Early Cretaceous transtension and transpression during arc building in Central Chile: evidence from mafic dike swarms, *Andean Geol.* 38, 37-63.
- Delouis, T. Monfret, L. Dorbath, M. Pardo, L. Rivera, D. Comte, H. Haessler, J.P. Caminade, L. Ponce, E. Kausel, A. Cisternas, (1997). The Mw = 8.0 Antofagasta (northern Chile) earthquake of 30 July 1995: A precursor to the end of the large 1877 gap. *Bulletin of the Seismological Society of America*, 87 (2): 427–445. doi: <https://doi.org/10.1785/BSSA0870020427>.
- Delouis, B., J.M. Nocquet, M. Vallée (2010). Slip distribution of the February 27, 2010 Mw = 8.8 Maule Earthquake, central Chile, from static and high-rate GPS, InSAR, and broadband teleseismic data, *Geophys. Res. Lett.*, 37, L17305, doi:10.1029/2010GL043899.
- Demets, C., R. Gordon, D. Argus, S. Stein, (1990). Current Plate Motions. *Geophysical Journal International*. 101– 425 - 478. 10.1111/j.1365-246X.1990.tb06579.x.
- Espinoza, M., Montecino, D., Oliveros, V., Astudillo, N., Vásquez, P., Reyes, R., Celis, C., González, R., Contreras, J., Creixell, C., Martínez, A., (2019). The synrift phase of the early Domeyko Basin (Triassic, northern Chile): Sedimentary, volcanic, and tectonic interplay in the evolution of an ancient subduction-related rift basin. *Basin Research* 31, 4-32.
- Farías M., D. Comte D., S. Roecker, D. Carrizo, M. Pardo, (2011). Crustal extensional faulting triggered by the 2010 Chilean Earthquake: The Pichilemu Seismic Sequence: *Tectonics*, v. 30, TC6010, doi:10.1029/2011TC002888. Farrar, A.D., Cooke, D.R., Hronsky, J.M.A., Wood, D.G., Benavides, S., Cracknell, M.J., Banyard, J.F., Gigola, S., Ireland, T., Jones, S.M., Piquer, J., (2023). A Model for the lithospheric architecture of the Central Andes and the localization of giant porphyry copper deposit clusters. *Economic Geology* 118 (6), 1235–1259, doi: 10.5382/econgeo.5010.



- 680 Fedotov, S. A., (1968). On seismic cycle, possibility of quantitative seismic regionalization and long-term seismic prediction. In *Seismic Zoning of the USSR* (ed. S. Medvedev) (Nauka, Moscow) pp. 121-150.
- Fischer, T., (2021)., Control estructural sobre la circulación de magmas y fluidos hidrotermales Miocenos y Cuaternarios en el sector de La Invernada, Región del Maule, Chile. Valdivia: Universidad Austral de Chile, 314.
- Forsyth, D. W., Yang, M.D. Mangriotis, Y. Shen, (2003). Coupled seismic slip on adjacent oceanic transform faults. *Geophysical Research Letters*, 30(12).
- 685 Fujie, G., S. Kodaira, Y., Kaiho, et al., (2018). Controlling factor of incoming plate hydration at the north-western Pacific margin. *Nat Commun* 9, 3844.
- Gana, P., R. Wall, A. Gutiérrez, (1996). Mapa Geológico del Área de Valparaíso – Cuaracaví. Regiones de Valparaíso y Metropolitana, Mapas Geológicos N°1, Escala 1:100.000. Servicio Nacional de Geología y Minería, Chile.
- 690 Geersen, J., C. Ranero, U. Barckhausen, U., (2015). Subducting seamounts control intraplate coupling and seismic rupture in the 2014 Iquique earthquake area. *Nat Commun* 6, 8267. <https://doi.org/10.1038/ncomms9267>.
- Glodny, J., H. Echtler, S. Collao, M. Ardiles, P. Burón, O. Figueroa, (2008): Differential Late Paleozoic active margin evolution in South-Central Chile (37°S-40°S) -The Lanalhue Fault Zone. *Journal of South American Earth Sciences*, 26, 4, 397-411 DOI: 10.1016/j.jsames.2008.06.001.
- 695 Gutscher M.A., J. Malavieille, S. Lallemand, J.Y. Collot, (1999). Tectonic segmentation of the north Andean margin: impact of the Carnegie Ridge collision, *Earth and Planetary Science Letters*, 168, 255-270.
- Haberland, C., A. Rietbrock, D. Lange, K. Bataille, S. Hofmann, (2006). Interaction between forearc and oceanic plate at the south-central Chilean margin as seen in local seismic data. *Geophysical Research Letters* 33: 1-5.
- Hansen, S., B. Schmandt, A. Levander, et al., (2016). Seismic evidence for a cold serpentinized mantle wedge beneath Mount
700 St Helens. *Nat Commun* 7, 13242. <https://doi.org/10.1038/ncomms13242>
- Hayes, G., (2018). Slab2 – A Comprehensive Subduction Zone Geometry Model: U.S. Geological Survey data release, <https://doi.org/10.5066/F7PV6JNV>
- Hayes, G., M. Herman, W. Barnhart, et al., (2014). Continuing megathrust earthquake potential in Chile after the 2014 Iquique earthquake. *Nature* 512, 295–298. <https://doi.org/10.1038/nature13677>
- 705 Heidarzadeh, M., Murotani, S., Satake, K., Ishibe, T., Gusman, A.R., (2016). Source model of the 16 September 2015 Illapel, Chile Mw 8.4 earthquake based on teleseismic and tsunami data. *Geophys. Res. Lett.* 43, 643–650.
- Hyndman R.D., S. M. Peacock, (2002). Serpentinization of the forearc mantle, *Earth and Planetary Science Letters* 212, 417-432.
- Kay, S.M., Mpodozis, C., (2002). Magmatism as a probe to the Neogene shallowing of the Nazca plate beneath the modern
710 Chilean flat slab. *Journal of South American Earth Sciences* 15, 39-57.
- Kimura G., A. Yamaguchi, M. Masataka, (2018). Upper-plate tectonic hysteresis and segmentation of the rupture area during seismogenesis in subduction zones—A case study of the Nankai "rough", *Geology and Tectonics of Subduction Zones: A*



Tribute to Gaku Kimura, Timothy Byrne, Michael B. Underwood, III, Donald Fisher, Lisa McNeill, Demian Saffer, Kohtaro Ujiie, Asuka Yamaguchi, [https://doi.org/10.1130/2018.2534\(05\)](https://doi.org/10.1130/2018.2534(05)).

- 715 J. Kley, C.R. Monaldi, J.A. Salfity. (1999). Along-strike segmentation of the Andean foreland: causes and consequences, *Tectonophysics*, Volume 301, Issues 1–2, Pages 75-94, ISSN 0040-1951, [https://doi.org/10.1016/S0040-1951\(98\)90223-2](https://doi.org/10.1016/S0040-1951(98)90223-2).
- Kohler, P. A., (2016). *Geología 29odelling29 del Complejo Volcánico Laguna del Maule y su control sobre la deformación cortical 29odell*. Undergraduate thesis. Concepción: Universidad de Concepción, 225.
- Koper, K. D., A. R. Hutko, T. Lay, and O. Sufri, (2012). Imaging short-period seismic radiation from the 27 February 2010
720 Chile (Mw 8.8) earthquake by back-projection of P, PP, and PKIKP waves, *J. Geophys. Res.* 117, B02308
- Lamb, S. and P. Davis. (2003). Cenozoic climate change as a possible cause for the rise of the Andes. *Nature*. 425. 792-7. [10.1038/nature02049](https://doi.org/10.1038/nature02049).
- Lanza, F., A. Tibaldi, F.L. Bonali, C. Corazzato, (2013). Space–time variations of stresses in the Miocene–Quaternary along the Calama–Olacapato–El Toro Fault Zone, Central Andes. *Tectonophysics* 593, 33-56.
- 725 Lara, L., A. Lavenu, J. Cembrano, C. Rodríguez, C., (2006). Structural controls of volcanism in transversal chains: resheared faults and neotectonics in the Cordón Caulle–Puyehue area (40.5°S), Southern Andes. *Journal of Volcanology and Geothermal Research* 158, 70–86, <https://doi.org/10.1016/j.jvolgeores.2006.04.017>.
- Lay, T., H. Kanamori and L. Ruff, (1982). The asperity model and the nature of large subduction zone earthquake occurrence, *Earthquake Prediction Research*, 1, 3-71.
- 730 Lay, T., and S. L. Bilek, (2007). Anomalous earthquake ruptures at shallow depths on subduction zone megathrusts, in: *The Seismogenic Zone of Subduction Thrust Faults*, Edited by T. H. Dixon and J. C. Moore, Columbia University Press, New York, pp. 476-511.
- Lay, T., C. J. Ammon, H. Kanamori, K. D. Koper, O. Sufri, and A. R. Hutko, (2010). Teleseismic inversion for rupture process of the 27 February 2010 Chile (Mw 8.8) earthquake, *Geophys. Res. Lett.*, 37, L13301, doi:10.1029/2010GL043379.
- 735 Lay, T., H.E.E Yue, E. E. Brodsky, and C. An, (2014). The 1 April 2014 Iquique, Chile Mw 8.1 earthquake rupture sequence, *Geophys. Res. Lett.*, 41, doi:10.1002/2014GL060238
- Lay, T., (2015). The surge of great earthquakes from 2004 to 2014, *Earth and Planetary Sci. Lett.*, Invited Frontiers Paper, 409, 133-146.
- Lee, S.J., T.Y. Yeh, T.C. Lin, Y.Y. Lin, T.R. Song, B.S. Huang, , (2016), Two-stage composite megathrust rupture of the 2015
740 Mw8.4 Illapel, Chile, earthquake identified by spectral-element inversion of teleseismic waves, *Geophys. Res. Lett.*, 43, 4979–4985, doi:10.1002/2016GL068843.
- Li, L., T. Lay, K. F. Cheung, and L. Ye, (2016). Odellingdeling of teleseismic and tsunami wave observations to constrain the 16 September 2015 Illapel, Chile, MW 8.3 earthquake rupture process, *Geophysical Research Letters*, 43, 4303-4312, doi:10.1002/2016GL068674



- 745 Lin, Y. N. N., A. Sladen, F. Ortega-Culaciati, F., M. Simons, J.P. Avouac, E.J., Fielding, A. Socquet, (2013). Coseismic and postseismic slip associated with the 2010 Maule Earthquake, Chile: Characterizing the Arauco Peninsula barrier effect. *Journal of Geophysical Research: Solid Earth*, 118(6), 3142-3159.
- Lorito, S., F. Romano, F., S. Atzori, et al., (2011). Limited overlap between the seismic gap and coseismic slip of the great 2010 Chile earthquake. *Nature Geosci* 4, 173–177 <https://doi.org/10.1038/ngeo1073>.
- 750 Loveless, J. P., & Meade, B. J. (2011). Stress modulation on the San Andreas fault by interseismic fault system interactions. *Geology*, **39**, 1035–1038. <https://doi.org/10.1130/G32215.1>
- Lutz, B.M., Axen, G.J., van Wijk, J.W., Phillips, F.M., (2022). Whole-lithosphere shear during oblique rifting. *Geology* 50, 412–416, <https://doi.org/10.1130/G49603.1>.
- Maekawa H., M. Shzui, T. Ishii, P. Freyer, J.A. Pearce, (1993). Blueshist metamorphism in active subduction zone, *Nature*,
755 v. 364, p. 520-523.
- Marrett, R.A., R.W. Allmendinger, R.N. Alonso, R.E. Drake, (1994). Late Cenozoic tectonic evolution of the Puna Plateau and adjacent foreland, northwestern Argentine Andes. *Journal of South American Earth Sciences*, Vol. 7, N°2, pp179-207.
- Mccaffrey, R., Stein, S., & Freymueller, J. (2002). Crustal block rotations and plate coupling. *Geodynamics Series*, **30**, 101–122.
- 760 McCuaig, T.C., Hronsky, J.M.A., (2014). The mineral system concept: the key to exploration targeting. *Society of Economic Geologists*, Special Publication 18, 153-176.
- Melgar, D., W. Fan, S. Riquelme, J. Gengm C. Liang, M. Fuentes, G. Vargas, R. M., Allen, P. M. Shearer, and E. J. Fielding, (2016). Slip segmentation and slow rupture to the trench during the 2015, Mw8.3 Illapel, Chile earthquake, *Geophys. Res. Lett.*, 43, 961–966, doi:10.1002/2015GL067369
- 765 Melnick D., H.P. Echtler, (2006). Morphotectonic and Geological digital Map Compilations of the South-Central Chile (36°-42°S), In *The Andes active subduction orogeny*, Onken et al. editors, *Frontiers in Earth Sciences*, ,565-568, Elsevier, 569p.
- Melnick, D. & B. Bookhagen, M. Strecker, H. Echtler, (2009). Segmentation of megathrust rupture zones from fore-arc deformation patterns over hundreds to millions of years, Arauco Peninsula, Chile. *Journal of Geophysical Research*. 114. 10.1029/2008JB005788.
- 770 Menant, A., S. Angiboust, T. Gerya, T. et al., (2020). Transient stripping of subducting slabs controls periodic forearc uplift. *Nat Commun* 11, 1823. <https://doi.org/10.1038/s41467-020-15580-7>.
- Mendoza, C., S. Hartzel, and T. Monfret, (1994). Wide-band analysis of the 3 March 1985 central Chile earthquake: Overall source process and rupture history, *Bull. Seismol. Soc. Am.*, 84, 269–283.
- Métois, M., A. Socquet, C. Vigny, , (2012). Interseismic coupling, segmentation and mechanical behavior of the Central Chile
775 subduction zone. *Journal of Geophysical Research*. 117. 10.1029/2011JB008736.
- Métois, M., Vigny, C., & Socquet, A. (2016). Interseismic Coupling, megathrust earthquakes and seismic swarms along the Chilean Subduction Zone (38°–18°S). *Pure and Applied Geophysics*, **173**, 1431–1449. <https://doi.org/10.1007/s00024-016-1280-5>



- Miller, N. C., D. Lizarralde, J.A. Collins, W.S. Holbrook, H.J. Van Avendonk, , (2021). Limited mantle hydration by bending
780 faults at the Middle America Trench. *Journal of Geophysical Research: Solid Earth*, 126, e2020JB020982.
<https://doi.org/10.1029/2020JB020982>
- Moggi, K. (1977). Seismic activity and earthquake prediction, *Proc. Earthquake Pred. Res. Syrup.*, 1976, 203-214, Tokyo.
- Moggi, K., (1985), *Earthquake Prediction* (Academic Press, Tokyo,).
- Moreno, M., Rosenau, M., & Oncken, O. (2010). 2010 Maule earthquake slip correlates with pre-seismic locking of Andean
785 subduction zone. *Nature*, **467**, 198–202. <https://doi.org/10.1038/nature09349>
- Moreno, M., D. Melnick, M. Rosenau, J. Baez, J. Klotz, O. Oncken, et al., (2012). Toward understanding tectonic control on
the Mw 8.8 2010 Maule Chile earthquake. *Earth and Planetary Science Letters*, 321, 152-165.
- Molina, D., A. Tassara, R. Abarca, R., D. Melnick, A. Madella, (2021). Frictional segmentation of the Chilean megathrust
790 from a multivariate analysis of geophysical, geological, and geodetic data. *Journal of Geophysical Research: Solid Earth*, 126,
e2020JB020647, <https://doi.org/10.1029/2020JB020647>.
- Moscoco, E., I. Grevemeyer, (2015). Bending-related faulting of the incoming oceanic plate and its effect on lithospheric
hydration and seismicity: A passive and active seismological study offshore Maule, Chile. *Journal of Geodynamics*. 90. 58-
70. [10.1016/j.jog.2015.06.007](https://doi.org/10.1016/j.jog.2015.06.007).
- Mpodozis, C., V. Ramos, (1990). *The andes of Chile and Argentina*. Circum Pacific Council Publications.
- 795 Müller, R. D., S. Zahirovic, S.E. Williams, J., Cannon, M. Seton, D.J. Bower, M.G. Tetley, C. Heine, E. Le Breton, S. Liu, S.,
S.H.J. Russell, T. Yang, J., Leonard, J., and M. Gurnis, (2019). A global plate model including lithospheric deformation along
major rifts and orogens since the Triassic. *Tectonics*, vol. 38,
- Nealy, J. L., M. W. Herman, G. L. Moore, G. P. Hayes, H. M. Benz, E. A. Bergman, and S. E. Barrientos (2017). 2017
Valparaíso earthquake sequence and the megathrust patchwork of central Chile, *Geophysical Research Letters* 44, doi:
800 [10.1002/2017GL074767](https://doi.org/10.1002/2017GL074767).
- Niemeyer, H., H. Berríos, R. de la Cruz, (2004). Temperatures of formation in Triassic cataclasites of Cordillera Domeyko,
Antofagasta, Chile. *Rev. Geol. Chile* 31, 3-18.
- NOAA National Centers for Environmental Information. (2022): ETOPO 2022 15 Arc-Second Global Relief Model. NOAA
National Centers for Environmental Information. [Dataset]. DOI: [10.25921/fd45-gt74](https://doi.org/10.25921/fd45-gt74)
- 805 Okada, Y. ,(1985). Surface Deformation due to Shear and Tensile Faults in a Half-Space. *Bulletin of the Seismological Society
of America*, 75, 1135-1154
- Palacios, C., Ramírez, L.A., Townley, B., Solari, M., Guerra, N., (2007). The role of the Antofagasta–Calama Lineament in
ore deposit deformation in the Andes of northern Chile. *Mineralium Deposita* 42, 301-308.
- Pasten-Araya, F., P. Salazar, S. Ruiz, E. Rivera, B. Potin, A. Maksymowicz,, et al., (2018). Fluids along the plate interface
810 influencing the frictional regime of the Chilean subduction zone, northern Chile. *Geophysical Research Letters*, 45.
<https://doi.org/10.1029/2018GL079283>.



- Peacock S.M., (1993). Large-scale hydration of the lithosphere above subducting slabs, *Chemical Geology*, Volume 108, Issues 1–4, Pages 49-59, ISSN 0009-2541, [https://doi.org/10.1016/0009-2541\(93\)90317 C](https://doi.org/10.1016/0009-2541(93)90317 C).
- Pearce, R.K., A. Sánchez de la Muela, M. Moorkamp, J.O.S Hammond, T.M. Mitchell, J. Cembrano, J. Araya-Vargas, P.G.Meredith, P. Iturrieta, N. Pérez-Estay, N.R. Marshall, J. Smith, G. Yáñez A. Griffith, W., C. Marquardt, A. Stanton-Yonge, R. Núñez, (2020). Reactivation of fault systems by compartmentalized hydrothermal fluids in the Southern Andes revealed by magnetotelluric and seismic data. *Tectonics* 39, e2019TC005997, .
- Peña, M., 2022. Origen de las Rotaciones Tectónicas en el Márgen Occidental de América del Sur: Influencia de Heterogeneidades en las Placas de Nazca y Sudamericana. Tesis para Optar al Grado de Doctor en Ciencias, Mencion Geología. Inédito, 214 p. Universidad de Chile, Facultad de Ciencias Físicas Y Matemáticas, Departamento de Geología. Chile.
- Perrin, C., Waldhauser, F., & Scholz, C. H. (2021). The shear deformation zone and the smoothing of faults with displacement. *Journal of Geophysical Research: Solid Earth*, 126, e2020JB020447. <https://doi.org/10.1029/2020JB020447>
- Philibosian, B., A.J. Meltzner, (2020). Segmentation and supercycles: A catalog of earthquake rupture patterns from the Sumatran Sunda Megathrust and other well-studied faults worldwide. *Quaternary Science Reviews* 241, <https://doi.org/10.1016/j.quascirev.2020.106390>.
- Piquer, J., Skármeta, J., Cooke, D.R., (2015). Structural evolution of the Río Blanco-Los Bronces district, Andes of central Chile: controls on stratigraphy, magmatism and mineralization. *Economic Geology* 110, 1995-2023.
- Piquer, J., R.F. Berry, R.J. Scott, D.R. Cooke, (2016). Arc-oblique fault systems: their role in the Cenozoic structural evolution and metallogenesis of the Andes of central Chile. *Journal of Structural Geology* 89, 101–117, <https://doi.org/10.1016/j.jsg.2016.05.008>.
- Piquer, J.; G. Yáñez, O. Rivera, D. Cooke, (2019). Long-lived damage zones associated with fault intersections in the Andes of Central Chile. *Andean Geology* 46 (2): [doi:http://dx.doi.org/10.5027/andgeoV46n2-3106]
- Piquer J., O. Rivera, G. Yáñez, N. Oyarzun, (2021a). The Piuquencillo Fault System: a long-lived, Andean-transverse fault system and its relationship with magmatic and hydrothermal activity, *Solid Earth*, (<https://doi.org/10.5194/se-2020-142>).
- 835 Piquer, J., P. Sanchez-Alfaro, P. Pérez-Flores, P., (2021b). A new model for the optimal structural context for giant porphyry copper deposit formation. *Geology* 49, 597-601, <https://doi.org/10.1130/G48287.1>.
- Poli P., A. Maksymowicz, S. Ruiz (2017). The Mw 8.3 Illapel earthquake (Chile): Preseismic and postseismic activity associated with hydrated slab structures. *Geology*. 45. [10.1130/G38522.1](https://doi.org/10.1130/G38522.1).
- Pritchard, M.E., M. Simons, P.A. Rosen, S. Hensley, F.H. Webb, (2002), Co-seismic slip from the 1995 July 30 Mw= 8.1 Antofagasta, Chile, earthquake as constrained by InSAR and GPS observations. *Geophysical Journal International*, 150: 362-376. <https://doi.org/10.1046/j.1365-246X.2002.01661.x>.
- Radic, J.P., (2010). Las cuencas cenozoicas y su control en el volcanismo de los Complejos Nevados de Chillán y Copahue-Callaqui (Andes del Sur, 36-39° S). *Andean Geology* 37 (1): 220-246. Doi: [10.5027/andgeoV37n1-a09](https://doi.org/10.5027/andgeoV37n1-a09).
- Ramos, V., (2008). The Basement of Central Andes: The Arequipa and Related Terranes. *Annu. Rev. Earth Planet. Sci.*, 36, pp. 289-324.
- 845



- Ramos, V., S. Kay, (2006). Overview of the tectonic evolution of southern central Andes of Mendoza and Neuquén (35°-39° S latitude). Geological Society of America, Special Paper 407.
- Ranero C. & V. Sallares. (2004). Geophysical evidence for hydration of the crust and mantle of the Nazca plate during bending at the north Chile Trench. *Geology*. 32. 10.1130/G20379.1.
- 850 Richards, J.P., Jourdan, F., Creaser, R.A., Maldonado, G., DuFrane, S.A., (2013). Geology, geochemistry, geochronology, and economic potential of Neogene volcanic rocks in the Laguna Pedernal and Salar de Aguas Calientes segments of the Archibarca lineament, northwest Argentina. *Journal of Volcanology and Geothermal Research* 258, 47–73.
- Rivera, O., 2017. Geodynamic Setting for Porphyry Copper Deposits in Central Chile: Role of Translithospheric Structures and Gravimetric Anomalies in Andean Metallogeny. Master Thesis, Department of Geological Sciences, Faculty of
855 Engineering and Geological Sciences. Catholic University of the North, Chile 215 pp.
- Rivera, O., J. Cembrano, (2000). Modelo de Formación de Cuencas Volcano-Tectónicas en Zonas de Transferencia Oblicuas a la Cadena Andina: El Caso de las Cuencas Oligo-Miocenas de Chile Central y su Relación con Estructuras WNW-NW (33°00' – 34°30' LS). In: 9° Congreso Geológico Chileno, Actas, vol. N°2, p. 631-636, Puerto Varas.
- Roquer, T., G. Arancibia, J. Rowland, P. Iturrieta, D. Morata, J. Cembrano, (2017). Fault-controlled development of shallow
860 hydrothermal systems: structural and mineralogical insights from the Southern Andes. *Geothermics* 66, 156-173, <http://dx.doi.org/10.1016/j.geothermics.2016.12.003>.
- Roland, E. and J.J. McGuire, (2009), Earthquake swarms on transform faults. *Geophysical Journal International*, 178: 1677-1690. <https://doi.org/10.1111/j.1365-246X.2009.04214.x>
- Ruegg, J.C., J. Campos, R. Armijo, S. Barrientos, P. Briole, R. Thiele, R., et al., (1996). The Mw = 8.1 Antofagasta earthquake
865 of July 30 1995: first results from teleseismic and geodetic data. *Geophys. Res. Lett.* 23 (9), 917–920.
- Ruiz, S., R. Madariaga, (2018). Historical and recent large megathrust earthquakes in Chile. *Tectonophysics*. <http://dx.doi.org/10.1016/j.tecto.2018.01.015>.
- Ruiz, S., R. Madariaga, M. Astroza, G.R. Saragoni, M. Lancieri, C. Vigny, J. Campos, (2012). Short Period Rupture Process of the 2010 Mw 8.8 Maule Earthquake in Chile. *Earthquake Spectra*, Vol 28, N.S1, S1-S18
- 870 Ruiz, S., M. Metois, A. Fuenzalida, J. Ruiz, F. Leyton, R. Grandin, C. Vigny, R. Madariaga, J. Campos, (2014). Intense foreshocks and a slow slip event preceded the 2014 Iquique Mw 8.1 earthquake. *Science*, 345, 1165-1169, DOI: 10.1126/science.1256074.
- Ruepke, L., J. Morgan, M. Hort, J. Connolly, (2004). Serpentine and the subduction water cycle. *Earth and Planetary Science Letters*. 223. 17-34. 10.1016/j.epsl.2004.04.018.
- 875 Salfity, J. A. (1985). Lineamentos transversales al rumbo andino en el Noroeste Argentino. In: IV Congreso Geológico Chileno, Antofagasta, Chile, Vol. 2, pp. 119–137.
- Saffer, D.M. & H. Tobin, (2011). Hydrogeology and Mechanics of Subduction Zone Forearcs: Fluid Flow and Pore Pressure. *Annu. Rev. Earth Planet. Sci.*. 39. 157-186. 10.1146/annurev-earth-040610-133408.



- Safer, D. M., (2017). Mapping fluids to subduction megathrust locking and slip behavior: Fluids and Subduction Megathrust
880 Locking, *Geophys Res Lett* 44, 9337–9340.
- Sagripanti, L., Folguera, A., Gimenez, M., Rojas Vera, E.A., Fabiano, J.J., Molnar, N., Fennell, L., Ramos, V.A., (2014).
Geometry of Middle to Late Triassic extensional deformation pattern in the Cordillera del Viento (Southern Central Andes): a
combined field and geophysical study. *J. Iber. Geol.* 40, 349-366.
- Saillard, M., L. Audin, B. Rousset, J.-P. Avouac, M. Chlieh, S. R. Hall, L. Husson, and D. L. Farber (2017). From the seismic
885 cycle to long-term deformation: linking seismic coupling and Quaternary coastal geomorphology along the Andean
megathrust, *Tectonics*, 36, doi:10.1002/2016TC004156.
- Sandwell, D. T., Müller, R. D., Smith, W. H., Garcia, E., & Francis, R. (2014). New global marine gravity model from CryoSat-
2 and Jason-1 reveals buried tectonic structure. *Science*, 346(6205), 65-67.
- Santibáñez I., J. Cembrano, T. García-Pérez, C. Costa, G. Yáñez, C. Marquardt, G. Arancibia, G. González, (2019). Crustal
890 faults in the Chilean Andes: geological constraints and seismic potential, *Andean Geology*, 46 (1): 32-65. Doi:
10.5027/andgeoV46n1-3067.
- Satake, K., M. Heidarzadeh, (2017). A Review of Source Models of the 2015 Illapel, Chile Earthquake and Insights from
Tsunami Data. In: Braitenberg, C., Rabinovich, A. (eds) *The Chile-2015 (Illapel) Earthquake and Tsunami*. Pageoph Topical
Volumes. Birkhäuser, Cham. https://doi.org/10.1007/978-3-319-57822-4_1.
- 895 Scholz C. H., (1990). *The Mechanics of Earthquakes and Faulting* (2nd Edition), Cambridge University Press, 504p.
- Scholz, C. H., and J. Campos, (2012). The seismic coupling of subduction zones revisited, *J. Geophys. Res.*, 117, B05310,
doi:10.1029/2011JB009003.
- Schurr, B., G. Asch, M. Rosenau, R. Wang, O. Oncken, S. Barrientos, P. Salazar, and J.-P. Vilotte, (2012). The 2007M7.7
Tocopilla northern Chile earthquake sequence: Implications for along-strike and down-dip rupture segmentation and megathrust
900 frictional behavior, *J. Geophys. Res.*, 117, B05305, doi:10.1029/2011JB009030.
- Schurr, B., G. Asch, S. Hainzl, S. et al., (2014). Gradual unlocking of plate boundary controlled initiation of the 2014 Iquique
earthquake. *Nature* 512, 299–302 <https://doi.org/10.1038/nature13681>
- SERNAGEOMIN, (2003). *Mapa Geológico de Chile 1:1.000.000: digital version*. Servicio Nacional de Geología y Minería,
Digital Geological Publication No. 4 (CD-ROM, version 1.0). Santiago, Chile.
- 905 Shillington, D., A. Bécnel, M. Nedimović, Et al., (2015). Link between plate fabric, hydration and subduction zone seismicity
in Alaska. *Nature Geosci* 8, 961–964. <https://doi.org/10.1038/ngeo2586>
- Sibson, R.H., (1990). Conditions for fault-valve behavior, in Knipe, R.J., and Rutter, E.H., eds., *Deformation Mechanisms,
Rheology and Tectonics: Geological Society [London] Special Publication 54*, p. 15–28,
<https://doi.org/10.1144/GSL.SP.1990.054.01.02>.
- 910 Sibson, R.H., (2020). Preparation zones for large crustal earthquakes consequent on fault-valve action. *Earth, Planets and
Space* 72:31, <https://doi.org/10.1186/s40623-020-01153-x>.



- Sielfeld, G., D. Lange, J. Cembrano, (2019). Intra-Arc Crustal Seismicity: Seismotectonic Implications for the Southern Andes Volcanic Zone, Chile. *Tectonics* 38, 552–578, <https://doi.org/10.1029/2018TC004985>.
- Stanton-Yonge, A., W.A. Griffith, J. Cembrano, R. St. Julien, P. Iturrieta, (2016). Tectonic role of margin-parallel and margin-
915 transverse faults during oblique subduction in the Southern Volcanic Zone of the Andes: Insights from boundary element
350delling: *Tectonics* 35, 1990–2013, <https://doi.org/10.1002/2016TC004226>.
- Talwani P., (2014). *Intraplate Earthquakes*, Cambridge University press, 360p.
- Thingbaijam K. K. S., P. M. Mai, K. Goda, (2017). New Empirical Earthquake Source-Scaling Laws. *Bulletin of the
Seismological Society of America*; 107 (5): 2225–2246. Doi: <https://doi.org/10.1785/0120170017>.
- 920 Torres, J., (2021). Caracterización del lineamiento Laguna fea-volcán san Pedro, región del Maule: Relación con actividad
magmática e hidrotermal. Undergraduate thesis. Valdivia: Universidad Austral de Chile, 174.
- Tsuji, T., J. Ashi, Y. Ikeda, Y., (2014). Strike-slip motion of a mega-splay fault system in the Nankai oblique subduction zone.
Earth Planet Sp 66, 120. <https://doi.org/10.1186/1880-5981-66-120>.
- Vigny, C., A. Socquet, S. Peyrat, J.C. Ruegg, M. Métois, R. Madariaga, et al., (2011). The 2010 Mw 8.8 Maule Megathrust
925 Earthquake of Central Chile, Monitored by GPS, *Science*, 1417-1421, 332, 6036, American Association for the Advancement
of Science, doi: 10.1126/science.1204132.
- Wall, R., P. Gana, A. Gutiérrez, (1996). Mapa Geológico del Área de San Antonio- Melipilla. Regiones de Valparaíso,
Metropolitana y del Libertador Bernardo O'Higgins. Mapas Geológicos N°2, Escala 1:100.000. Sernageomin, Chile.
- Wall, R., D. Sellés, P. Gana, (1999). Geología del Área Tilttil-Santiago, Región Metropolitana de Santiago. Serie Mapas
930 Geológicos N°11, Escala 1:100.000. Sernageomin, Chile.
- Wallace, L. M., Beavan, J., McCaffrey, R., & Darby, D. (2004). Subduction zone coupling and tectonic block rotations in the
North Island, New Zealand. *Journal of Geophysical Research*, 109, B12406. <https://doi.org/10.1029/2004JB003241>
- Wang, K. & S.L. Bilek, (2011). Do subducting seamounts generate or stop large earthquakes? *Geology* 39, 819–822.
- Wdowinski, S., (1992). Dynamically supported trench topography, *J. Geophys. Res.*, 97(B12), 17651– 17656,
935 doi:10.1029/92JB01337.
- Wiemer, D., Hagemann, S.G., Hayward, N., Begg, G.C., Hronsky, J., Thébaud, N., Kemp, A.I.S., Villanes, C., (2023). Cryptic
trans-lithospheric fault systems at the western margin of South America: implications for the formation and localization of
gold-rich deposit superclusters. *Frontiers in Earth Science* 11, 1159430, doi: 10.3389/feart.2023.1159430.
- Xia, S., J. Sun, H. Huang, (2015). Degree of serpentinization in the forearc mantle wedge of Kyushu subduction zone:
940 quantitative evaluations from seismic velocity. *Marine Geophysical Research*, 36, 101-112.
- Yañez, G., P. Gana, R. Fernández, (1998). Sobre el origen y significado geológico de la anomalía Melipilla, zona central de
Chile. *Revista Geológica de Chile*, 25, No. 2, 175-198.
- Yañez, G., C.R. Ranero, R. Von Huene, J. Díaz, (2001). Magnetic anomaly interpretation across the southern central Andes
(32°-34°S): The role of the Juan Fernandez Ridge in the late Tertiary evolution of the margin. *Journal of Geophysical Research*.
945 106, 6325-6345



Yañez G., J. Cembrano, (2004). The role of the viscous plate coupling in the late tertiary Andean deformation. *Journal of Geophysical Research*, vol 106, 6325-6345, 2004.

Yañez G., O. Rivera, (2019). Crustal dense blocks in the fore-arc and arc region of Chilean ranges and their role in the magma ascent and composition. *Breaking paradigms in the Andean metallogeny, Journal of South American Earth Sciences*, 93, pp. 950 51-66. DOI: 10.1016/j.jsames.2019.04.006.

Yue L.T., , E. Brodsky, C. An, (2014). The 1 April 2014 Iquique, Chile, Mw 8.1 earthquake rupture sequence, *Geophys. Res. Lett.*, 41, 3818– 3825, doi:10.1002/2014GL060238.

Zienkiewicz, O. C., and R. L. Taylor (1991), *The Finite Element Method*, vol. 2, *Solid and Fluid Mechanics Dynamics and Non-linearity*, 4th ed., McGraw-Hill, New York.

955